Convection in porous media

A numerical study of a side heated cavity with spatially varying conductivities using the conjugate heat transfer model.

by

R. Koolstra

to obtain the degree of Master of Science
at the Delft University of Technology,
to be defended publicly on October 24 , 2019 at 09:30 AM.

Student number:	4475933		
Project duration:	Februari 1, 2018 – October, 2019		
Thesis committee:	dr. ir. S. Kenjeres,	TU Delft,	Supervisor
	M. Chakkinghal,	TU Delft,	Daily supervisor
	Dr.ir. M.J.B.M. Pourquie,	TU Delft	
	dr.ir. D. Lathouwers,	TU Delft	

TU Delft

Abstract

Porous media are used for a wide variation of applications in energy production and storage. One of those applications is the storage of heat which are of great importance in the renewable energy transition. Most literature reported limit itself only to one single thermal conductivity for the porous media. In reality however, the porous media often consist of multiple materials with different conductivities. This thesis researches numerically natural convective heat transfer in a porous media with both conductive and insulating objects.
The porous medium is simplified to a side heated cavity filled with water as fluid (Pr = 7), 32 aluminum objects with a thermal conductivity ratio of $\lambda^* = \frac{\lambda_{Al}}{\lambda_f} = 337.33$ and 32 wooden objects at thermal conductivity ratio $\lambda^* = \frac{\lambda_W}{\lambda_f} = 0.29$. 4 cases, each with the aluminum and wooden cubes differently configured are simulated at a Rayleigh number(Ra) of $10^5, 10^6$ and 10^7. Conjugate heat transfer (the fluid fase and solid fase are modelled as separate regions) simulations are done with direct Navier-Stokes where $Ra = 10^5$ and 10^6 are run steady and $Ra = 10^7$ is run transient. There are two different geometries simulated. One when the objects are unattached (heat cannot directly conduct into the objects from the walls) to the wall and when they are attached (heat can directly conduct into the objects) to the wall. From these simulations the temperature profile, the velocity field and the Nu profile is obtained. Also the average Nu at the hot wall and the U_{rms} are calculated and compared between the different cases. Lastly the thermal disequilibrium $\%|DT|$ between the solid temperature and fluid temperature is calculated and compared between place of the object in the cavity and between the cases.
The simulations show that conductive objects increased heat transfer at $Ra = 10^5$ when they are close to the wall. This is because they decrease the thermal resistance heat travels in the thermal boundary layer. Insulating objects on the other hand show decreased heat transfer as they increase the thermal resistance in the thermal boundary layer. At $Ra = 10^6$ and at $Ra = 10^7$ the circulation is to strong and the thermal boundary layer is mostly in between the wall and the objects so there is little difference seen in the flow and heat transfer.
When the objects are attached to the wall the simulations show very different results for the flow and heat transfer and is very dependent on the conductivity and position of the object. Conductive objects attached at the wall, especially at the bottom of the wall where the temperature-gradient is the biggest, greatly improve the flow and heat transfer. They improve the area heat is transported from the wall to the fluid and thus increase the buoyancy force significantly. Insulting objects attached to the wall on the other hand prevent heat from flowing through the object and also prevents flow from reaching the wall. A big decrease in velocity and heat transfer is seen for all Ra values. For a case where conductive objects are placed against the wall and there are insulating objects in the middle, heat transfer can be improved compared to a fluid-only cavity for $Ra \geq 10^6$

Preface

This thesis has been written by me as graduation project for my study. But I wouldn't have done it if wasn't for my friends, family and research group around me so I want to take this chance to thank them. First and mostly I want to thank Manu for daily supervising me. Your feedback has taught me almost from scratch how to do numerics. I want to thank Sasa and Chris for guiding me at the process meetings and Julia and Nima, who did similar topics for lending their knowledge.
I want to thank everyone in the research group of transport phenomena for helping me when I had questions but also for making this group a pleasant home for me to work in. I want to thank Matheus, Elin and Xiaolin for always hanging out with me, during office hours and outside of them. I had some fun times.
I am grateful for my family: my parents and my brother that I could come home and de-stress myself and that you guys were always interested in my progress even though it was slow sometimes. My thanks goes to my friends at Wolbodo for creating a nice place were I could enjoy myself during these last years.
Last but not least I want to thank Luders, Kristina, Bhavya and Kiana for proofreading my report. Without you this report wouldn't be as beautiful as it is now.

R. Koolstra
Delft, October 2019

Contents

List of Figures

List of Tables

Nomenclature

Acronyms

BL	Boundary layer
DT	Thermal disequilibrium

Non-dimensionless numbers

Pr	Prandtl number
Ra	Rayleigh number
Nu	Nusselt number
Re	Reynolds number

Symbols

U_{RMS}	RMS of the velocity through out the cavity.	
ρ	Density	m/s^2
c_p	Specific heat capacity under constant pressure	J/kgK
λ	Thermal conductivity	W/mK
λ^*	Relative thermal conductivity λ_s/λ_l	
α	Diffusive heat constant $k/\rho c_p$	m^2/s
ν	Kinematic viscosity	m^2/s
μ	Dynamic viscosity	
β	Thermal expansion coefficient	$1/K$
T	Temperature	K
ΔT	Temperature difference $T_h - T_c$	K
L	Length of cavity	m
W	Width of cavity	m
H	Height of cavity	m
p	Pressure	N/m^2
N	Number of objects in the cavity, Number of faces of cell, Number of cells	
K	Permeability	
u	Velocity vector	
u	Velocity in x direction	m/s^2
v	Velocity in y direction	m/s^2
w	Velocity in z direction	m/s^2

u^*	Normalized velocity $u^* = \frac{\sqrt{u^2+v^2+z^2}L}{Ra^{3/7}\alpha}$	
q	Heat flux	W/m^2
$/phi$	Intensive property	
S	Production	
Γ	Diffusion constant	
V	Volume	m^3
A	Surface area	m^2
α_p	Under relaxation factor	
δ	Boundary layer thickness	m
$< Nu >$	Average Nu at the hot wall	W/m^2

Subscripts

f	fluid, face of cell
s	solid
c	cold
h	hot
0	initial state, only fluid-case
T	thermal
v	viscous
av	average
i, j	index notation
w	west face
e	east face
W	west node
E	east node
P	center node
al	aluminium
w	wood
99	99% of mean.
atm	atmosphere

1 Introduction

Global warming is one of the biggest problems humanity faces this day and finding alternative methods of energy production and reduction of energy consumption is one of biggest technological challenges. An important form of alternative energy used is thermal energy. Understanding fundamentally how heat is transferred is useful for different kinds of sustainable applications such as producing thermal energy in solar receivers[1], storing energy in sensible or latent heat storage[2], dynamic insulating in houses[3] or geothermal energy [4]. Porous media are used in all these applications to control heat flow or store energy because they are good heat exchangers and are able to store heat.
When porous media are modelled in literature often a few assumptions are made. These assumptions include continuous liquid and solid phase of the porous media and a single conductivity for the solid phase[5]. However, these are not always good approximations. The porous medium in geothermal energy can have different materials and particle sizes and in pcm storage high conduction particles can be added to increase conductivity[1]. In other applications it can be interesting to play with different conductivities to see how they affect charge and discharge of heat. It is thus interesting to research how spatially varying objects with different conductivities influence the heat flow.

1.1. Heat transfer

There are three modes of heat transfer that can take place. The first mode is conduction. Heat or the kinetic energy of molecules is transferred from one molecule to the other via collisions or transfer of electrons. How well a material can conduct heat is often expressed in the thermal conductivity λ [W/mK]. Metals have mostly high conductivities because they can freely move electrons ($\lambda \sim 10-2000$). Gases and fluids conduct less heat and often have λ between 0.03 and 0.6 at room temperature as they solely depend on the collisions of molecules[6].
The second mode of transport is convection. This is the transfer of heat by movement of the molecules themselves and thus can only take place in fluids. An important form of convection is natural convection. As fluid gains more heat it will expand and become less dense than the fluid on top and rise upwards, this is called buoyancy. Natural convection is often expressed through the non-dimensional Rayleigh (Ra) number. A full description of the non-dimensional numbers used in this report can be found in Appendix B. Another useful non-dimensional number is the Nusselt (Nu) number. Nu expresses the ratio of convection over conduction. A high Nu thus means that the flow is convection dominated while a low Nu means that the flow is conduction dominated[6].
The third mode of heat transfer is radiation. With radiation, heat is transferred via photons. All objects radiate photons all the time and the frequency and energy of the photon is dependent to the fourth power to the absolute temperature of the object. If the temperature difference between two objects is small than the object receives approximately as much radiation as it emits. For this reason, radiation is neglected in this report. In porous media both convection and conduction are important as the fluid can convect heat while the objects can conduct heat[6].

1.2. Simplifications

The cases of thermal storage and geothermal energy production are very specific and hard to model. In this report we are only interested in how different materials influence the heat transfer so some simplifications are made. Figure 1.1 shows a hot reservoir to the left and a cold reservoir to the right with in the middle a reservoir filled with objects of different sizes and materials. Heat is transported from the left to the right. To make things simpler it is assumed that the hot and cold reservoir are so big that they will have a constant temperature over time. This means they can be modelled as a hot wall with constant temperature T_h and a cold wall with constant temperature T_c. Radiation is neglected for all cases in this report, this is valid for applications with small temperature differences as the radiation depends on the fourth power of the temperature and for cases with low emissivity coefficients. The next simplification is to only use two different conductivities instead of a large range to get only two kind of objects. One with a high relative conductivity (λ^*) compared to the fluid and one with a relative low conductivity. Aluminum is chosen as the high conductive material ($\lambda^* = 337.3$) and wood is chosen for the low conductive material ($\lambda^* = 0.29$). An aspect ratio of 1 for the volume is chosen.

Figure 1.1: Model of the ground with a hot heat reservoir and a cold reservoir. It is filled with objects of different size and material.

1.3. Model

The continuous solid phase model only assumes one effective conductivity over the whole control volume[5]. This makes it impossible to study the spatial differences of heat transfer different conductivities would create. So for this research the control volume is divided in solid regions and fluid region where the transport equations are solved separately. The objects are either made from aluminum or wood and are placed in 4 different configurations which can be seen in figure1.2. Water is chosen as the fluid because it has a conductivity in between wood and aluminum. The same configurations are repeated but then with the objects touching the walls so that heat can be transferred directly into and from the wall. A lot can be researched about these 4 cases so the study is limited to natural convection at a flow with a Ra of $10^5, 10^6$ and 10^7, which is in the laminar flow regime. Simulations at Ra 10^5 and 10^6 are done with steady state solvers as the results are time independent. Simulations done at 10^7 are done with a transient solver. ANSYS 17.1 will be used to solve the Navier-Stokes and energy equation.

1.4. Research goal

The main research question of this thesis is: how do spatially varying conductive objects influence natural convective heat flow? To research this the main question is divided in the following sub-questions:

1. How does a natural convective flow look like in a cavity filled with only fluid?
2. How do the 4 different arrangements in figure 1.2 influence the heat transfer and the flow compared to the only fluid case.
3. How do the 4 different arrangements influence the flow when objects touch the wall compared to the only fluid case?
4. How does the change in Ra influence the flow of the cases done in sub-questions 1 to 3?

The research questions will be answered by solving DNS simulations and analyzing the Temperature profiles, Velocity fields and Nu at the wall. Also there will be looked at the thermal disequilibrium of the objects closest to the wall.

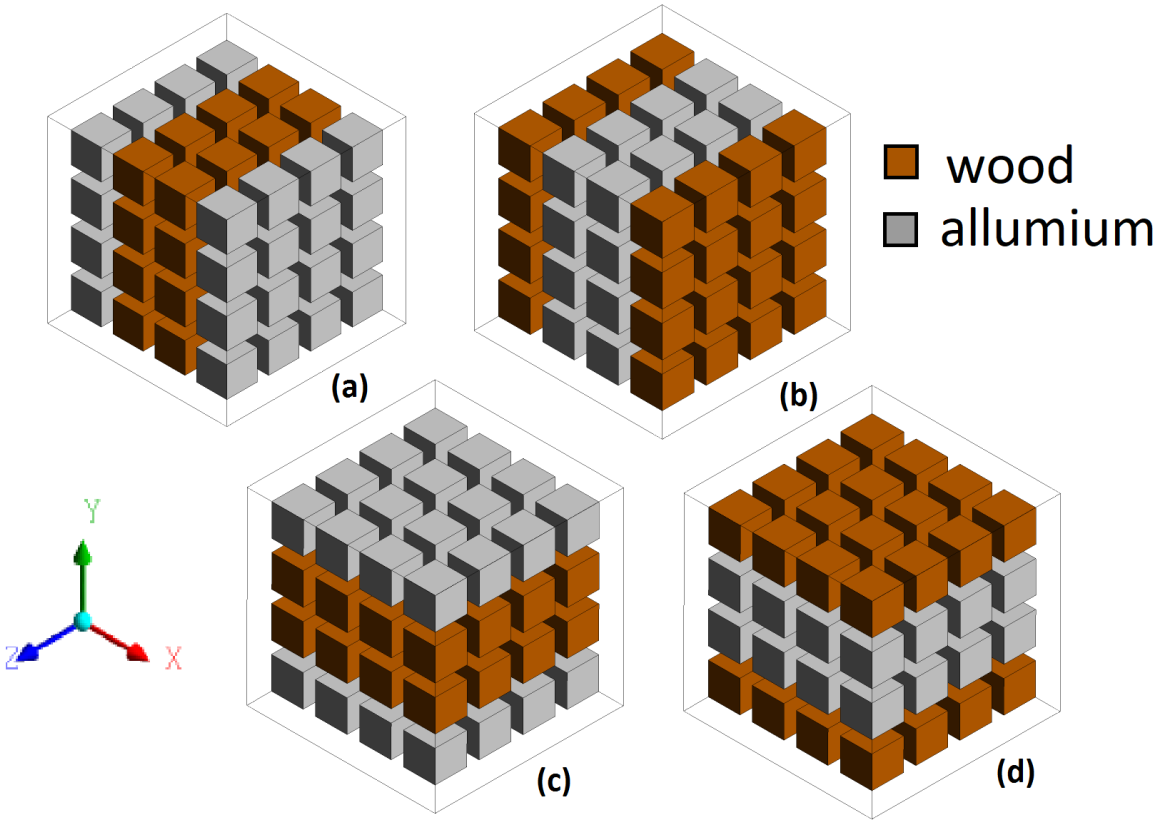

Figure 1.2: The four configurations used in this thesis.

1.5. Outline

In Chapter 2 the theory needed to understand the results will be explained. First a literature study will be conducted of previous studies this study builds on. After that information is given about natural convection in a cavity with only fluid and a cavity filled with objects. The Chapter ends with an explanation of the core transport equations the numerics are based on. In chapter 3 the numerical models are explained the boundary conditions are given and the meshes are shown. Also the convergence criteria are explained. In Chapter 4 the validation cases are discussed. In chapter 5 the results of Case A to D are discussed when the objects are when they are a distance from the wall and in chapter 6 the results of Case A to D when the objects are touching the wall are discussed. Chapter 7 contains the conclusion and in Chapter 8 some recommendations are made.

2 Theory

In this chapter the theory will be given. First, the results of the literature study conducted will be given and the research already done on this topic will be outlined. After which the theory of some subjects important to this report are given. In order: Natural convection in a cavity, natural convection in a medium with object(s), models for porous media, effective conductivity and the governing equations.

2.1. Introduction

In this thesis, the natural convection in a side heated cavity with a porous medium is investigated. In the past several experimental and numerical studies have been done on this topic. Most of the time when porous media is studied numerically, Darcy's law or Darcy's law with Forcheimer and Brinkham's extensions is applied. For one of these models to be applied, the pore length scale should be much smaller than the macroscopic flow length scale[7]. Another restriction for Daryc's law to be valid is that the Re and Pe should not exceed unity in the boundary layers and the characteristic grain diameter must be smaller than the boundary layer thickness[8].
Lauriat and Prasad did a numerical study of a sideheated porous medium using the Darcy's law with Forcheimer and Brinkham extentions to study porous media. They also found that the heat transfer rate increases as the conductivity ratio increases and that it is even possible to have a higher heat transfer rate with a porous medium than a only fluid case if the conductivity ratio and permeability are high enough[9].
Seki et al did an experimentally study with a differentially side heated porous medium. They used two different solids(iron balls or glass beads) and three different fluids(water, transformer oil and ethyl alcohol). They did the experiment for different Ra and aspect ratios (H/W) and found out that the Nu increases as Pr, Ra and H/W increases[10].
Iman et al. did an experimental study with a cavity packed with spheres. They varied the conductivity ratio's, sphere sizes and Ra. They also experimented on a case with a gap between the spheres and the wall greater than the viscous and thermal boundary layer. They found that having a gap between the wall and the objects results in a higher Nu because the objects don't block the flow in the boundary layer. This effect is most strong at low Ra. This is because at low Ra the flow length scales are larger compared to the pore length scale and thus without a gap the flow cannot penetrate easy[7].
Multiple people have done numerical studies on a cavity with one or multiple objects. Instead of using Darcy's law with Forcheimer and Brinkham's extensions they separated the solid and liquid domains and solved the Navier-Stokes and energy equation for these regions. These equations will be explained in section 2.6.
House et al.[11] did simulations with a conducting solid object in a cavity. They varied the size of the object, the Rayleigh number and the conductivity ratio between the object and the fluid. They found that for object sizes that are smaller than the stagnant core of the rotating fluid the Nusselt number doesn't change. If the body size is larger the Nusselt is heavily influenced by the conductivity ratio. A high ratio will suppress the heat transfer while a low ratio will enhance the convective heat flow.
Mousa[12] did the same thing with a adiabatic block in the middle. He found that for low Ra ($Ra < 10^4$) the heat transfer rate decreases as the object size increases. For relative high Ra ($Ra = 10^5, 10^6$) the maximum heat transfer rate increases as the object size increases. For higher Ra the object size has little influence on the heat transfer rate. Bhave et al.[13] investigated an adiabatic block in a cavity while changing the block size,

Pr and Ra. They found that the adiabatic block prevented vertical conduction through the stagnant core and thereby increasing the natural convection. For each Rayleigh and Prandtl number there is an optimal block size that roughly corresponds to the stagnant core size. Larger blocks will block the flow and thus reduce the natural convection.
Roslan et al[14] have research polygon shaped objects in a cavity. They varied the number of edges (N) of the polygon and found that for polygons with $N \geq 5$ the Nusselt and the conduction ratio becomes independent of N.
Merrikh and Lage[15] did a study with multiple square objects in a cavity. They varied the number of blocks and the conductivity ratio while keeping the solid volume percentage at 36 %. They found that at a certain minimum amount of blocks N_{min} the main fluid flow switches from near the wall to the first channel between objects. Sharply decreasing the heat transfer. Overall a higher number of objects will decrease the Nusselt. If the flow is switched to the channels ($N \geq N_{min}$) a higher conductivity ratio will increase the heat transfer. If the flow is still near the wall ($N \leq N_{min}$) a higher conductivity ratio will decrease the heat transfer.
Raji et al.[16] did a similar study of a sideheated cavity with either 1, 4, 16 or 64 blocks in it while the objects occupied the same volume percentage. They confirmed that the Nu is decreased as N increases. They also found that at Ra below 10^5 at a fixed thermal conductivity ratio the Nu will decrease with increasing number of blocks. Hooman and Merrikh[17] found a least square fitting for the Nusselt number as a function of the Rayleigh number, the number of objects in the cavity and the λ^*. The maximum error of the correlation is less than 30.5 % and an average error of 6.1 %.

$$Nu = 0.0155 Ra^{0.45} N^{-0.268} \lambda^{*0.073} \tag{2.1}$$

2.2. Natural convection in a cavity

Natural convection in cavities has been studied intensively[18–24] because it has many applications. The simplest case is a 2D square where two of the walls have either a fixed temperature or heat flux. Two main situations are defined. The first case has the top and bottom have a fixed temperature or heat flux, this case is called Rayleigh-Bénard convection. In the second case the sidewalls have a fixed temperature or heat flux, called a differentially side heated cavity. This report is about differentially side heated cavities.
Let us assume at t = 0 the cavity is filled with a fluid that has T_0. At t = 0 the hot wall gets temperature $T_h = T_0 + 0.5\Delta T$ and the cold wall gets temperature $T_c = T_0 - 0.5\Delta T$. At t > 0 the hot wall starts conducting heat to the fluid which will expand and starting to exert a buoyancy force on the fluid. This gives the fluid a momentum upwards which in turn gives the fluid an upwards velocity until it reaches the top of the cavity. Because of conservation of mass the fluid at the top is pushed to left. At the cold wall the fluid cools downs, contracts and gets a downwards momentum resulting in a downwards velocity. The combination of the vertical velocity's at the sidewalls created by buoyancy and the horizontal velocity due to conservation of mass will create a circular motion throughout the cavity (see figure 2.2). This creates a flow at the walls, which creates a boundary layer and a stagnant center.
There are two types of boundary layers, a viscous or momentum boundary layer and a thermal boundary layer. The viscous boundary layer thickness is defined as the distance from the wall the maximum velocity is reached and the thermal boundary layer is defined as the distance from the wall where the mean temperature of the cavity is reached. The boundary layer is the most important region of the cavity because there the highest temperature and velocity gradients and the buoyancy force are present. An easy way to characterize the boundary layer is with the Prandtl number, which is the ratio of the viscous diffusivity over the thermal diffusivity. A high Prandtl number means a larger momentum boundary layer while a low Prandtl number means a lower momentum boundary layer(see figure 2.1).
The whole flow can be characterized by three non-dimensionless numbers. The Rayleigh number, Prandtl number and the aspect ratio. A higher Rayleigh number means stronger buoyancy force. This corresponds to a smaller thermal boundary layer. With scaling analysis on cavity flow the relation of $\delta_T \sim HRa_H^{-1/4}$ for Pr at 1 or higher can be found[25]. The empty cavity can be expressed in the Nu number at the hot or cold wall. A higher Rayleigh number causes higher convection and thus a higher Nu number at the hot and cold walls. Through scaling analysis the following estimation for Nu as relation of Ra can be found: $Nu_{av} = 0.364 \frac{L}{H} Ra^{1/4}$[25]. Rounaghi[26] did an experimental study and found a relationship between Nu and Ra for a cavity with aspect ratio 1 and water as fluid (Pr = 0.67): $Nu_{av} = 0.25 Ra^{0.26}$.

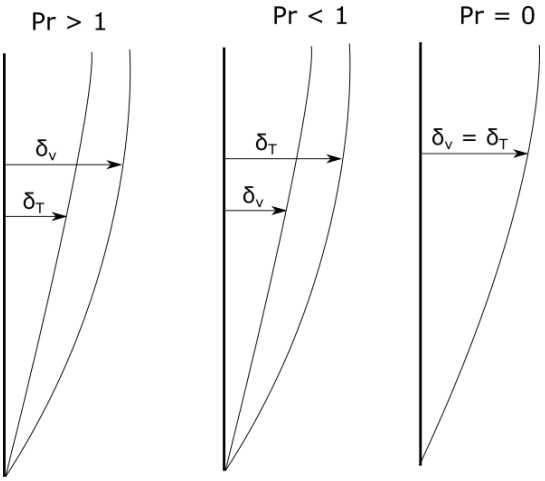

Figure 2.1: The Boundary Layer at different Pr values.

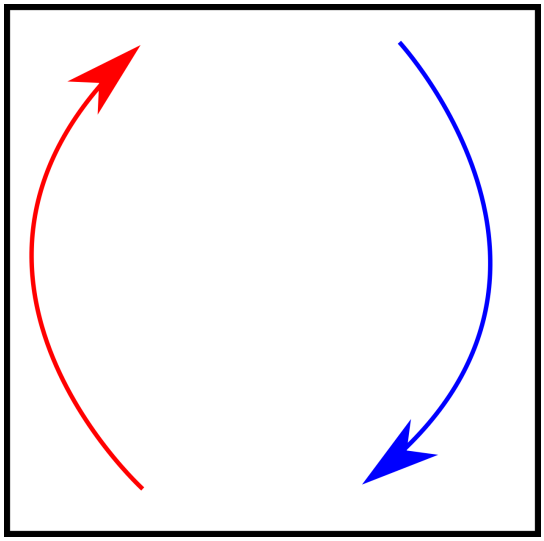

Figure 2.2: Natural convection in a cavity. The flow will circulate throughout the cavity due to the buoyancy force at the hot and cold wall.

2.3. Cavity with an object

House[11] was the first one to investigate how the heat transfer flows in a side heated cavity when there is an object in the middle. He did numerical investigations between $10^3 > Ra > 10^6$ and varied the relative body size from 0 to 1, where 0 is a cavity with only fluid and at 1 a body size the size of the cavity. He also varied the relative conductivity λ^*. As explained in the previous section, the flow in a side heated cavity is at the walls and the center is stagnant. The stagnant center becomes bigger as Ra increases. House found out that if the object in the middle of the cavity is not bigger than this stagnant center the object hardly has any influence at all. This is because most heat is transported via convection through the flow and the flow doesn't reach the object.

When the object is about as big as the stagnant center it starts to interact with the flow and two things can happen. If $\lambda^* < 1$ the heat transfer becomes bigger while if $\lambda^* > 1$ the heat transfer becomes smaller. This is because in an only fluid cavity there is still some conduction from the top to the bottom of the cavity, practically short circuiting the cavity and reducing the horizontal heat transfer. If there is an insulating object in the middle, this conduction from top to bottom is reduced and there is more heat transfer transferred through convection from the left wall to the right[13]. With an conducting object, the situation is reversed. Conduction from top to bottom is improved and more heat will be transported from top to bottom instead of left to right[11]. (see figure 2.3). The higher the Ra the less conduction plays a role and there is less difference in between relative conductivities.

If the object becomes bigger than the stagnant core it starts to reduce the flow significantly and with it the convective heat flow. This has especially effect on moderate and high Ra where the main form of heat transfer is convection.

2.4. Cavity with multiple objects

Merrikh and Lage[15] did a numerical study were they increased the number of blocks. For a small amount of objects the flow prefer to stay close to the wall leaving the fluid in between the objects mostly stagnant. But as the number of blocks increases the objects occupy space closer to the walls and start to penetrate the viscous boundary layer the flow starts to prefer the channel in between the first two columns closest to the wall. The number of objects needed to switch flows gets higher as Ra increases because higher Ra means a smaller viscous layer. This effect can be seen in figure 2.4. At Ra = 10^6 the flow switches at 32 objects while at Ra = 10^7 an the flow switches at 64 objects.

Merrikh and Lage also investigated the influence of the relative conductivity on the flow. A high λ^* will have two effects on the flow when there are a lot of objects in the cavity. Firstly it will increase the diffusion of heat at the wall through the conductive objects. this will increase the region the buoyancy force acts and increase the convective flow, especially at low Ra. On the other side high λ^* increase conduction from the top to the

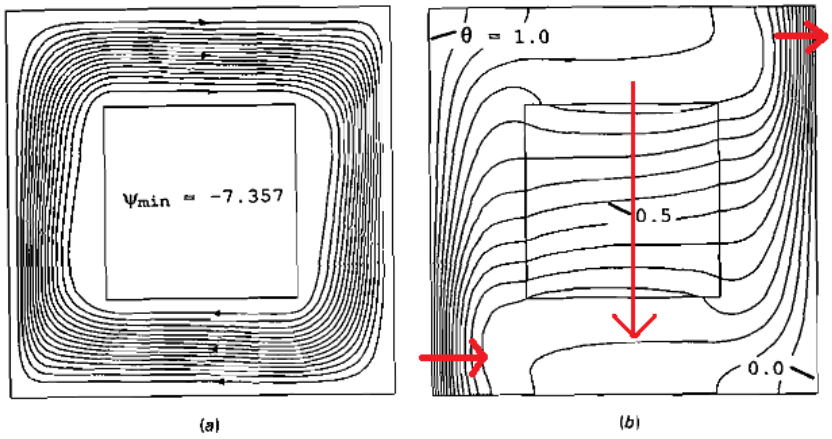

Figure 2.3: (a) Stream lines and (b) isotherms at side heated cavity of Ra = 10^5 and $\lambda^* = 0.2$. Simulation and images performed by House[11]. The red arrows in (b) show the direction of conduction in the cavity and how conductive objects can stimulate conduction from the top to the bottom.

bottom and decrease the overall heat transfer. In figure 2.5 it can be seen that for Ra = 10^6 with 36 objects and for Ra = 10^7 with 64 objects, both had the flow in the channel in between the first two objects, the heat transfer increases with λ^*. While the case of Ra = 10^7 with 32 blocks, which had the flow at the wall, the heat transfer decreases with λ^*. This shows that the objects have to be close enough to the wall for them to be surrounded by the flow to help (or prevent) the diffusion of heat and increase the buoyancy region. It also shows that the increase of the buoyancy region due to the conductive objects increases the heat transfer more than that the conduction from the top to the bottom decreases heat transfer.

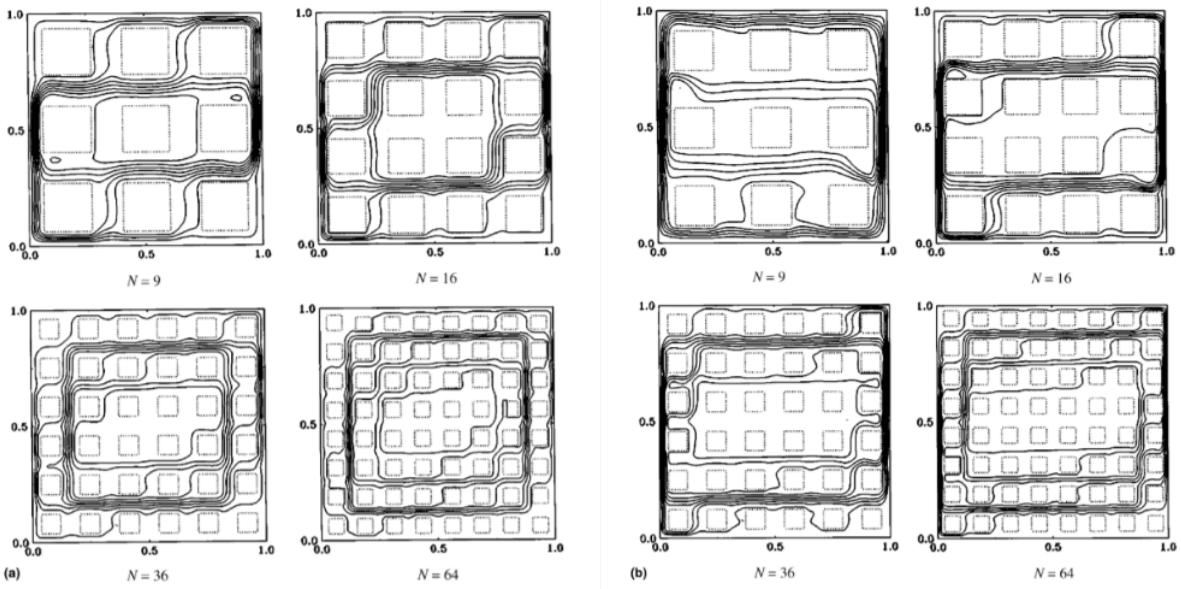

Figure 2.4: Cavity with 9, 12, 36 and 64 objects at a) Ra = 10^6 and b) Ra = 10^7. Simulations and pictures done by Merrikh and Lage [15].

2.5. Models for porous media

A porous media is defined as a solid structure with a lot of pores inside, either because it is composed out of a lot of grains or it is a solid skeleton with pores. It can be very useful for heat transfer applications as heat can be moved both through the solid and fluid. If the pore scale is much larger than the macroscopic flow the flow domain can be divided in elements and the porous medium can be approximated as a continuous medium. This makes modeling a lot easier. For this to be possible the elements must be much smaller than

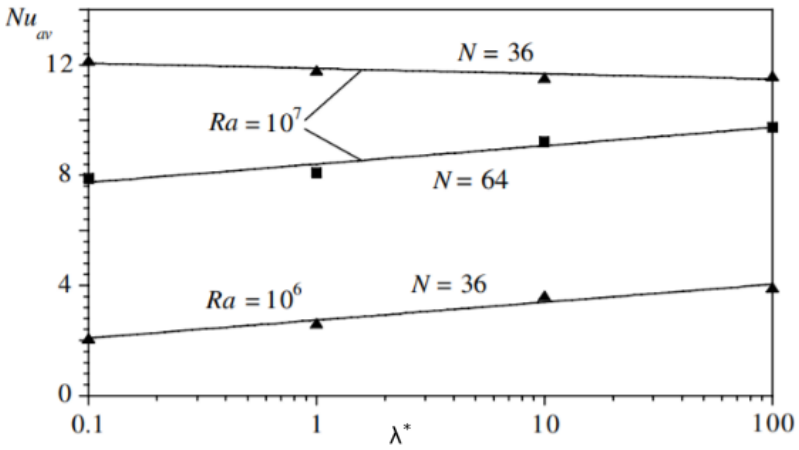

Figure 2.5: Average Nu plotted against λ^* at $Ra = 6$ and $Ra = 7$. Simulations and picture done by Merrikh and Lage [15].

the flow domain but much bigger than the pore scale. In those elements all parameters (velocity, density, temperature etc) are averaged(called a representative element volume)[27]. In this way the porous medium can be expressed as a continuous volume without having to look at all small fluctuations at the pore scale.
Darcy did experiments on flow in porous media and found a relationship between the pressure gradient and the velocity[27]:

$$u_i = -\frac{K}{\mu}\frac{\partial P}{\partial x_i} \tag{2.2}$$

where K is the permeability of the porous medium, μ the viscosity of the fluid and u the seepage velocity (the velocity through the porous medium, not the velocity of the fluid itself.) The Darcy equation is proven to be true by many experiments as long as the pore scale is small enough and the seepage velocity is small because the Darcy equation neglects the effect of solid boundaries of the grains and the inertial force of the fluid. To compensate for this, the Forheimer extension of the Darcy equation takes into the account the inertial force and the Brinkman version of the Darcy equation takes into effect of the solid boundaries of the grains[27]. None of those models are however used in this report as we are interested in the physics at the pore scale.

2.6. Governing equations

In natural convection there are three important equations. The continuity equation (2.3), the Navier Stokes equation (2.4) and the energy equations (2.5). In this report it is assumed that the flow is newtonian and incompressible. Also the Boussinesq approximation is used. A full derivation of these equations can be found in Appendix A. The continuity equation is defined as:

$$\frac{\partial u_j}{\partial x_j} = \frac{\partial u}{\partial x} + \frac{\partial v}{\partial y} + \frac{\partial w}{\partial z} = 0 \tag{2.3}$$

It states that mass is conserved in a certain volume. In our case a small piece of fluid we will call a fluid particle. Because the fluid is incompressible the divergence of the flow is always zero, everything that goes in to volume also come out the volume.
The Navier-Stokes equation is defined as:

$$\underbrace{\rho\frac{\partial u_i}{\partial t}}_{\text{change in momentum}} + \underbrace{u_j\frac{\partial u_i}{\partial x_j}}_{\text{advection}} = -\underbrace{\frac{\partial P}{\partial x_i}}_{\text{pressure}} + \underbrace{\mu\frac{\partial^2 u_i}{\partial x_j^2}}_{\text{viscosity}} + \underbrace{\beta(T_\infty - T)g_i}_{\text{buoyancy}} \tag{2.4}$$

This is a momentum balance on the fluid particle and has five terms. The first term is the change of momentum in time in the fluid particle. The second term is the advection (incoming and outgoing mass) of fluid through the fluid particle. The third term is the pressure on the fluid particle. The fourth force is the

viscous force on the fluid particle is the force that drags neighboring fluid along and is diffusive in nature. The last term are the body forces, in the case of natural convection this is the buoyancy force.
The last equation is the energy equation. It is the balance of internal energy in a fluid particle and can be transformed to its temperature format:

$$\underbrace{\rho c_P \frac{\partial T}{\partial t}}_{\text{change in temperature}} + \underbrace{\rho c_P u_j \frac{\partial T}{\partial x_j}}_{\text{convection}} = \underbrace{k \frac{\partial^2 T}{\partial x_j^2}}_{\text{conduction}} + \underbrace{q'''}_{\text{production}} \tag{2.5}$$

It consists of four terms. The first term is the temperature change in the fluid particle. The second term is the movement of mass at certain temperature which is called convective heat transfer. The third term is the diffusion of the temperature which is called conduction. And the last term is the production of heat in the fluid particle. In this report there is not a source that creates heat so q''' is 0.
By solving these three equations with the appropriate boundary conditions the temperature, velocity and pressure can be obtained at every point in space and time. However, solving these equations analytically is only possible for easy problems. For the rest of the problems, like the ones solved in this report, it is possible to discretize the problem and solve it numerical. This is further explained in Chapter 3.

3

Numerics

3.1. Volume difference scheme

Problems often are too complex to solve analytical. But the problems can still be solved by finding an approximate numerical solution. Numerical problems can be solved by discretization the volume in either points (finite difference method), elements (finite element method) or volumes (finite volume method). Table 3.1 shows which schemes are used during this research. for Ra = $10^5, 10^6$ steady state schemes are used while for Ra = 10^7 transient schemes are used.

Table 3.1: The different schemes used.

Equation	Steady state numerical schemes	Transient numerical schemes
Pressure-Velocity coupling	Simplec	Piso
Gradient	Least squares cell based	Least squares cell based
Pressure	Presto!	Presto!
Momentum	Second order upwind	Bounded second differencing
Energy	Second order upwind	Bounded second differencing
Transient	-	Bounded second order implicit.

All schemes are based on the finite volume method. This method is used because in transport phenomena it is fairly easy to divide the geometry in volumes and integrate the conservation laws discussed in section 2.6 on these volumes. These volumes are so small that it can be assumed that the solution is linearly within the cell. An example how the volume is split in 2D can be seen in figure 3.1. The goal is to find the temperature, pressure and velocity at the node points (red dots). First, the general conservation law is integrated.[28]

$$\int_V \frac{\partial \rho \phi}{\partial t} \mathrm{d}V + \oint \rho \phi u_j \mathrm{d}A_j = \oint \Gamma \frac{\partial \phi}{\partial x_j} \mathrm{d}A_j + \int_V S \mathrm{d}V \tag{3.1}$$

The surface of the cell is composed out of a number of N flat surfaces. The surface integral thus can be solved by summing all the solutions of these flat surface integrals.

$$\frac{\partial \rho \phi_p}{\partial t} V + \sum_{i=1}^{N_{faces}} \rho \phi_{f,i} v_{f,j} A_{f,ij} = \sum_{i=1}^{N_{faces}} \Gamma \frac{\partial \phi_{f,i}}{\partial x_j} A_{f,ij} + SV \tag{3.2}$$

ϕ_P is the value at the node P while ϕ_f is the value at the face of the cell. A_f is the cell surface and r_i is the distance between cell P and the neighboring cell i. By replacing ϕ, Γ and S with the right variables the discretized forms of the continuity equation, momentum equation and energy equation can be made. Table 3.2 shows which variables need to be used for each respectable equation. The next sections will explain some of the schemes used.

Table 3.2: Values for ϕ, Γ and S to create the transport equations.

Equation	ϕ	Γ	S
Continuity equation	1	0	0
Momentum-x equation	u	μ	$\frac{\mathrm{d}P}{\mathrm{d}x}$
Momentum-y equation	v	μ	$\frac{\mathrm{d}P}{\mathrm{d}y} - g\beta\left(T_\infty - T\right)$
Momentum-z equation	z	μ	$\frac{\mathrm{d}P}{\mathrm{d}z}$
Energy equation	$c_p T$	k	0

3.2. Least square cell based scheme

Suppose you have a grid like in figure 3.1 and you want to calculate the gradient between ϕ_P and ϕ_1. If a linear gradient is assumed between two cells then:

$$\frac{\partial \phi_P}{\partial x_j} r_1 = \left(\phi_1 - \phi_P\right) = \Delta\phi_1 \tag{3.3}$$

This can be done for all the gradients to all the neighboring cells and put in a matrix of the form:

$$\frac{\partial \phi_P}{\partial x_j} r_i = \Delta\phi_i \tag{3.4}$$

It is possible to decompose the gradient in the x and y (and z in 3D) direction. Here they are called a (x-direction) and b (y-direction). The same can be done for the radius r_i.

$$(x_i - x_P)a + (y_i - y_P)b = \phi_i - \phi_P \tag{3.5}$$

$$\Delta x_i a + \Delta y_i b = \Delta\phi_i \tag{3.6}$$

a and b can be found by solving the weighted minimization problem[29].

$$\min_{a,b} \sum_{i=1}^{n} w_i [\Delta\phi_i - \Delta x_i a - \Delta y_i b]^2 \tag{3.7}$$

w_i is a matrix of weighting factors which are determined through the Gram-Schmidth process.[30] The minimums of a and b are found by taking the derive with respect to a and b which gives us two equations for two unknowns.

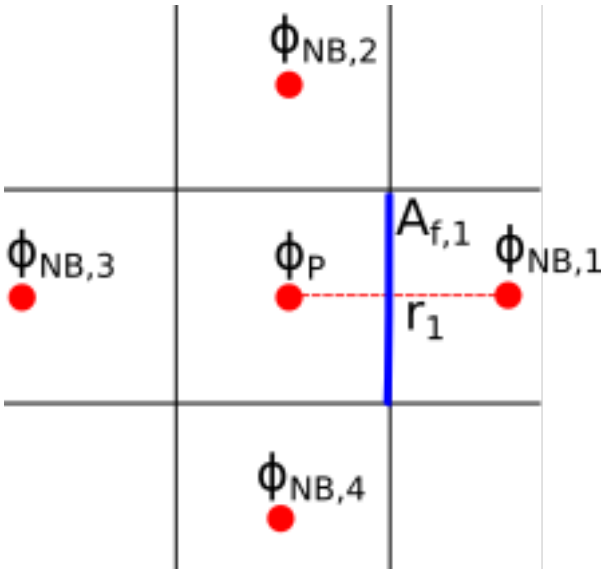

Figure 3.1: A scheme of how FVM works.

$$\frac{\mathrm{d}}{\mathrm{d}a}\sum_{i=1}^{n} w_i[\Delta\phi_i - \Delta x_i a - \Delta y_i b]^2 = 2\sum_{i=1}^{n} w_i[-\Delta\phi_i + \Delta x_i^2 a + \Delta x_i \Delta y_i b] = 0 \tag{3.8}$$

$$\frac{\mathrm{d}}{\mathrm{d}b}\sum_{i=1}^{n} w_i[\Delta\phi_i - \Delta x_i a - \Delta y_i b]^2 = 2\sum_{i=1}^{n} w_i[-\Delta\phi_i + \Delta x_i \Delta y_i a + \Delta y_i^2 b] = 0 \tag{3.9}$$

3.3. Second order upwind scheme

Solving the fluxes of the advection term through linear interpolation would however create numerical instabilities. This can be avoided by using the upwind scheme instead. The value of ϕ at the border of the volume would be assumed to be the same as the upstream node value[31] as sown in figure 3.2.

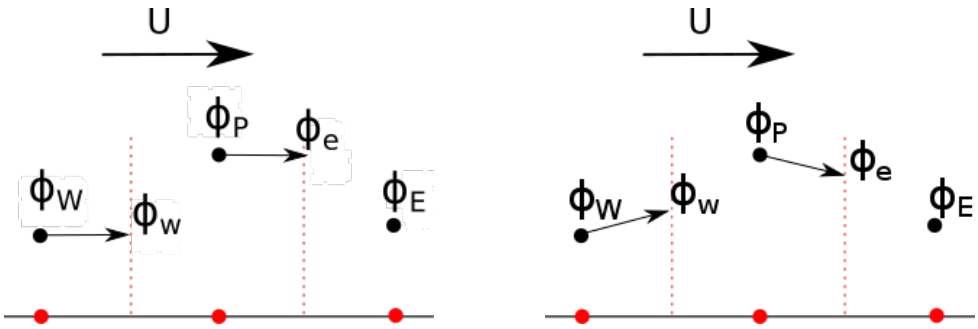

(a) first order upwind scheme (b) second order upwind scheme

Figure 3.2: 1D schematic of the (a)first and (b)second order upwind scheme

$$\phi_w = \phi_W \quad if \quad U > 0 \qquad \phi_w = \phi_P \quad if \quad U < 0 \tag{3.10}$$

$$\phi_e = \phi_P \quad if \quad U > 0 \qquad \phi_e = \phi_E \quad if \quad U < 0 \tag{3.11}$$

$$\tag{3.12}$$

In general terms it can be written as.

$$\phi_{f,i} = \phi_{u,i} \tag{3.13}$$

Where $\phi_{u,i}$ is the upstream value. Often only taking the upstream value is not vary accurate. To improve the accuracy without sacrificing the stability it is possible to add the first derivative of ϕ for a better guess. This is called second order upwind scheme.[32]

$$\phi_{f,i} = \phi_{u,i} + \nabla\phi_{u,i} \tag{3.14}$$

The derivative of ϕ at the center is calculated through the least square cell based scheme.

3.4. Bounded central differencing

Another way to determine the face value of ϕ is through central differencing which is the average of ϕ of the neighbouring cells plus their gradient:

$$\phi_w = \frac{\phi_W + \phi_P}{2} + \frac{\nabla\phi_W \cdot r_W + \nabla\phi_P \cdot r_P}{2} \tag{3.15}$$

Only doing central differencing gives very unstable results. Thus for bounded central differencing adjustments are made to make it bounded and prevent oscillating instabilities.[32]

3.5. Pressure term

The pressure is the source term in the momentum balance and when integrating the source term over the cell the pressure term can be described by:

$$\sum_{i=1}^{N_{faces}} p_f A_i \cdot \hat{\imath} \tag{3.16}$$

Here p_f is the pressure at the face. This can be calculated through linear interpolation. However, this gives can inaccurate results. Another way to calculate p_f is to use a separate grid that has its node points in the center of the faces of the original grid. A staggered grid. The Presto! scheme uses such a staggered grid to get accurate stable pressures without the need of interpolation. The downside is that it costs more computer resources as a second grid is used.[33]

3.6. Coupling scheme

To solve the Navier-Stokes the equation needs to be coupled to the continuity equation in so called pressure-velocity schemes. This is done by solving the pressure-correction equation. The most basic scheme is the SIMPLE scheme and works as followed[31]:

- Set up an initial pressure field p^*
- Solve the Navier-Stokes equations and obtain u^*, v^* and w^*
- solve the correction equations to obtain p', u', v' and w'.
- update the solution: $p = p^* + p'$, $u = u^* + u'$, $v = v^* + v'$ and $w = w^* + w'$
- Solve other equations like the energy equation to obtain T.
- Set $p = p^*$ and begin the next iteration.

The pressure-correction equation can give divergent results. It is thus important to use a under-relaxation factor:

$$p = p^* + \alpha_P p' \tag{3.17}$$

Where α_P is the under relaxation factor. Typically α_P is set to 0.1 or 0.2. SIMPLEC is variation on the SIMPLE scheme where the momentum equations are manipulated to allow for much a higher pressure underrelaxation parameter[34]. For the steady state simulations in this report the SIMPLEC scheme is used with $alpha_P$ set to 1. This results in much faster conversion rates. Piso is an extention to the SIMPLE scheme that allows for big time steps[34] and is therefore used in the transient schemes for the Ra = 10^7 simulations.

3.7. Geometry

Two slightly different geometries are used for all 4 cases. Both consists of an cavity with 64 solid objects in it. Half of the solid objects have the properties of wood (low conductivity) and the other half have the properties of aluminum (high conductivity). Water is used for the fluid in between the objects. Four cases have been investigated, each with different configurations of wood/aluminum solids. These cases can be seen in figure 1.2. The first geometry has an equal distance between the wall and the objects and the objects themselves. The second geometry has the nearest objects from the hot and cold wall attached to the wall. The geometries can be seen in fig 3.3 and a summery of their lengths can be seen in table 3.3.

Table 3.3: Nusselt numbers at the walls

geometry	geometry 1	geometry 2
L_{cavity}	0.101 m	0.101 m
L_{object}	0.017 m	0.017 m
L_{gap}	0.0066 m	0.011 m

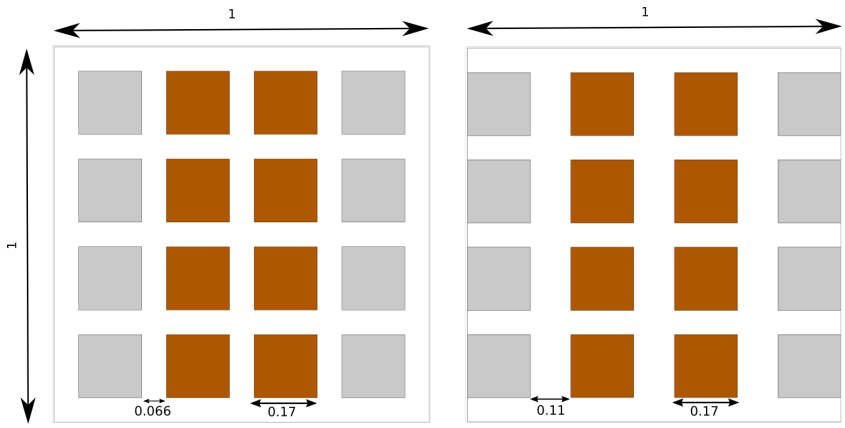

Figure 3.3: Length scales of the cases when the objects are a small distance from the wall(left) and when they are attached to the wall (right).

3.8. Boundary conditions and material properties

To fully specify the problem the right boundary conditions and initial conditions need to be applied. The following boundary conditions are applied:

Velocity boundary conditions

For velocity the no-slip and no-penetration boundary conditions are applied to all the present walls, both the walls from the cavity and those of the objects. No-slip boundary conditions means that there is no velocity parallel to the wall at the wall. No-penetration boundary condition means that there is no velocity perpendicular to the wall at the wall. Those two combined causes that there is no velocity at the walls:

$$\text{no slip} \quad \boldsymbol{u} = 0 \quad \text{at} \quad x/L = 0,1; \quad y/H = 0,1; \quad z/W = 0,1 \tag{3.18}$$

Temperature boundary conditions

The temperature boundary conditions are defined as follows. The left wall (hot wall) and right wall(cold wall) have fixed isothermal temperatures of T_h and T_c respectively. The other walls are adiabatic.

$$\text{left wall} \quad T = T_h \quad \text{at} \quad x = 0 \tag{3.19}$$

$$\text{right wall} \quad T = T_c \quad \text{at} \quad x/L = 1 \tag{3.20}$$

$$\text{other walls} \quad \frac{\partial T}{\partial x_j} = 0 \quad \text{at} \quad y/H = 0,1; \quad z/W = 0,1 \tag{3.21}$$

To make sure the heat transfer of the objects and the fluid is coupled, the heat flux at the solid-fluid interface is equal for both sides of the interface

$$\text{object walls} \quad \lambda_f \frac{\partial T}{\partial x_j} = \lambda_s \frac{\partial T}{\partial x_j} \tag{3.22}$$

Initial conditions

For the initial conditions a constant atmospheric pressure, zero velocity and a constant temperature gradient from the hot wall to cold the cold wall across the cavity is chosen. The temperature gradient is achieved by turning of the gravity and letting the simulation run a few iterations. By excluding the gravity the buoyancy force, which is the driving force of natural convection, doesn't play a role anymore and only conduction is left. The solution of this case is a better initial condition for temperature because it prevents very high temperature gradients at the cold and hot walls that appear when using a constant temperature as initial condition.

$$p = p_{atm} \tag{3.23}$$

$$\boldsymbol{u} = 0 \tag{3.24}$$

$$\frac{\partial T}{\partial x} = \frac{\Delta T}{L} \tag{3.25}$$

For Ra = 10^7 the simulations are first run at a steady state, after which that result is used as initial condition for running the transient schemes. This shortens the computing time considerable as the steady state schemes are much less process intensive.

Material properties

Table 3.4 shows the material properties used in the simulations.

Table 3.4: Operation parameters at 298 K and 1 atm

Parameter	value	unit
ρ_{water}	998	kg/m^3
$\rho_{aluminum}$	2719	kg/m^3
ρ_{wood}	700	kg/m^3
$c_{p,water}$	4182	J/kgK
$c_{p,aluminum}$	871	J/kgK
$c_{p,wood}$	2310	J/kgK
λ_{water}	0.6	W/mK
$\lambda_{aluminum}$	202.4	W/mK
λ_{wood}	0.173	W/mK
ν_{water}	1×10^{-6}	m^2/s
β	2.183×10^{-5}	1/K
g	-9.81	m/s^2
ΔT	1	K
Pr	6.99	-
Ra	$1.5 \times 10^5, 10^6, 10^7$	-

3.9. Mesh

The accuracy and validity of the simulation depends on the amount of cells and the quality of these cells. A coarse mesh will give inaccurate results while a fine mesh will cost a lot of computer resources and time. Thus it is important to find a fine balance between accuracy and computer resources. Bringing structure to the cells can help bring down the amount of cells needed for accurate results. One way to structure a mesh is by aligning the cells along the flow. This is wise because when a flow enters a cell with an angle it gives a numerical error that otherwise needs to be decreased by increasing the number of cells. Another way to increase efficient use of cells is to increase the cell amount in the boundary region and decrease it in the center. A high density of cells are only useful in high gradient regions and as explained in section 2.2 the boundary layer is the place with the high velocity and temperature gradient while the center is fairly isotropic. Three meshes are made for this study. Figure 3.4 shows the mesh the meshes made for these three studies. Mesh (a) is used for the validation case. Mesh (b) to study the effect of objects not attaching the walls and mesh(c) to study the effects of objects touching the wall. All meshes are done with hexahedron cells that are very thin at the border and become broader towards the center.

Two ways are used to find the amount of cells needed in the mesh. First an analytical estimation is made using a paper by Shishkina [35] for the amount of cells needed in the boundary layer. Then a mesh independent study is done to check if the mesh is indeed good enough. Shishkina et. al. [35] analytically estimated the minimum amount of cells needed in the boundary layer by solving the laminar Prandtl-Blasius equations for Rayleigh-Bénard convection. They found multiple relationships for the number of cells needed in the thermal and viscous boundary layer:

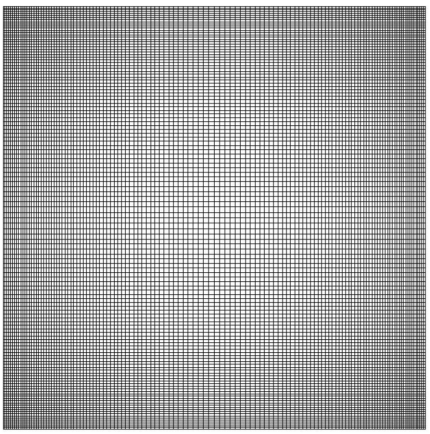

(a) Mesh of the validation cases.

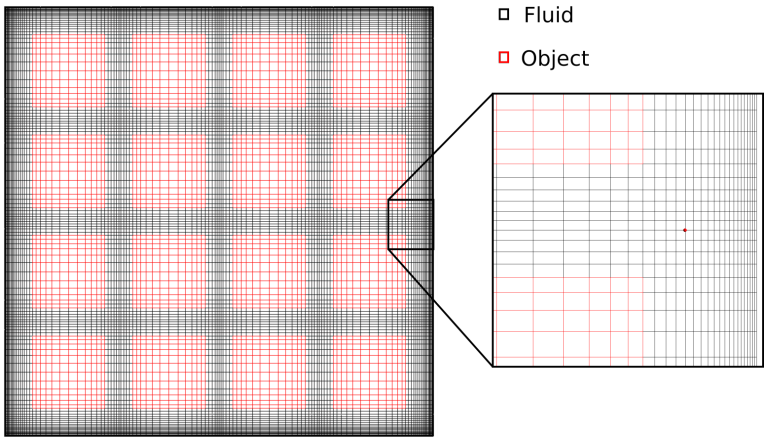

(b) Mesh with objects not attached to the walls.

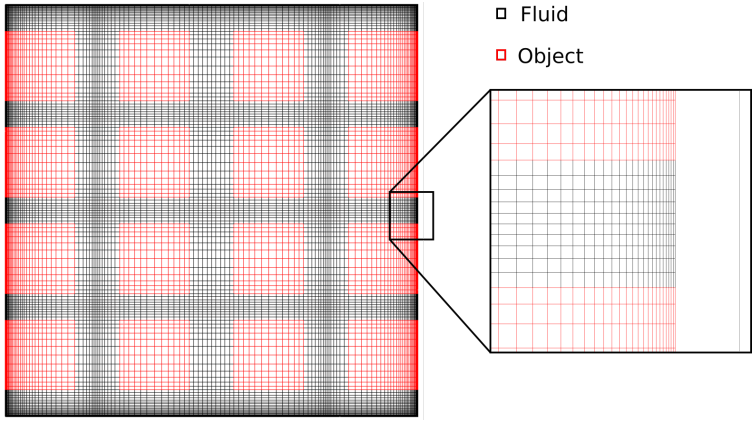

(c) Mesh with objects attached to the walls.

Figure 3.4: Cross-section of the three meshes used.

Table 3.5: Maximum number of cells needed in the boundary layer.

geometry	Validation Case	Objects don't touch the walls	Objects attached to the walls
Nu	10.2	8.3	5.6
$N_{th.BL}$	2.12	1.9	1.57
$N_{th.BL}$	4.13	3.72	3.06

$$N_{th.BL} = \sqrt{2Nu}E^{3/2}a \quad Pr > 3 \tag{3.26}$$

$$N_{v.BL} = \sqrt{2NuE}Pr^{1/3}a \quad Pr > 3 \tag{3.27}$$

Here, E is a constant of value : $E = 0.982$. a is empirical constant, obtained through experiments. Qiu Tong found a value for a based on experiments of Rayleigh-Bérnard convection in a cylindrical cell filled with water: $a \sim 0.482$. Table 3.5 gives the maximum of cells needed in the boundary layer for the simulations in this report.

A mesh independent study is done to check the validation of the mesh used. Table 3.6 shows the amount of cells and resulting Nu number of all the different cases.

When running Case A at Ra = 10^7 on the fine and the used mesh the average Nu number at the wall differed by 0.12% for the case when objects don't touch the wall and 0.9% for the case when the objects do touch the wall. This is within the limit to use the meshes.

Table 3.6: Number of cells in the various meshes

Mesh	course mesh	Used mesh	Fine mesh
Validation Case	-	$2.1 * 10^6$	-
Objects at a small distance from the walls	$2.1 * 10^5$	$1.6 * 10^6$	$3.3 * 10^6$
Objects attached to the walls	$2.2 * 10^5$	$2 * 10^6$	$5.5 * 10^6$

3.10. Convergence

To check how many iterations are needed to get an accurate result two things are measured. First of the residuals are measured. The residual is defined as:

$$R^{\phi} = \frac{\sum_{cellsP} |\sum_{nb} a_{nb}\phi_{nb} + b - a_P\phi_P|}{\sum_{cellsP} |a_{nb}\phi_{nb}|} \tag{3.28}$$

In a real system the property ϕ is conserved: $\sum_{nb} a_{nb}\phi_{nb} + b - a_P\phi_P = 0$. In a numerical system this is however not the case. But the closer the residual can be brought to 0 the better. Equation 3.28 sums up the residuals from all cells and scales them. The residuals are monitored and when they stop becoming smaller and vary around a stable very small value it is an indication the simulation is converged. An example of such a monitor can be seen in figure 3.5a.
The second method of checking whether the solution is converged is to monitor one of the parameters during the simulations. Because these are all steady state simulations all parameters should stop changing when the solution is converged. The Nu number at the hot wall and cold wall are monitored with the Nu number defined as:

$$< Nu_{wall} >= |\frac{< q_{wall} > * L}{\lambda * (T_{wall} - T_{mean})}| \tag{3.29}$$

Taking T_{mean} as reference temperature gives an identical Nu number for the cold and hot wall for a converged solution. Thus monitoring the Nu number gives two indications if the solution is converged. 1. The Nu number must not be changing anymore over iterations and 2. The Nu number at the hot and cold wall must be identical. The Nu monitored at the hot and cold wall of the validation case can be seen in figure 3.5b.

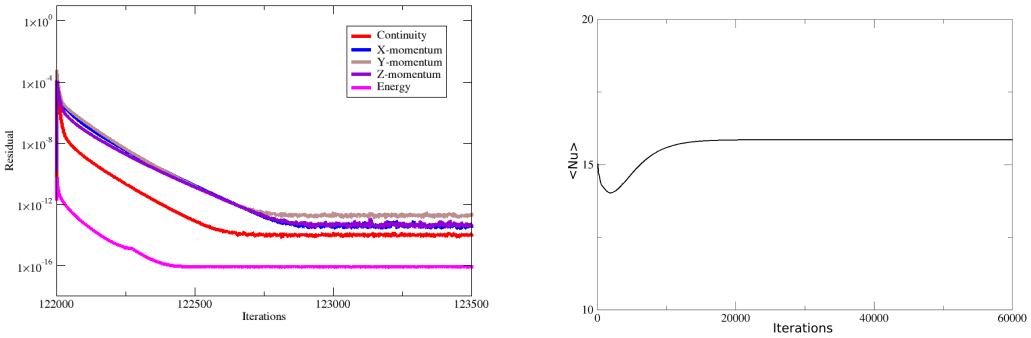

(a) Monitor of residuals of Case A with the objects not attached at Ra = 10^6

(b) Monitor of Nu number

Figure 3.5: Different convergence criteria through (a) Residuals and (b) Monitor of the Nu number

4

Validation

First a reference case: 'A cavity with only fluid', is analyzed. The temperature profiles and velocity fields can be seen in figure 4.2 & 4.3 respectively. As can be seen a big upward buoyancy force is created at the hot wall pushing the fluid up while at the cold wall the buoyancy force forces the fluid down. This creates a clockwise rotation of the fluid throughout the whole cavity. A boundary region is created at the hot and cold wall where the fluid is pushed up and down respectively. The higher the Rayleigh number the thinner the boundary layer but the higher the velocity within that boundary layer. Figure 4.4 shows the Nusselt number profile at the hot wall. As can be seen it increases for higher Rayleigh numbers indicating higher heat transfer. The heat transfer is highest near the bottom where the temperature gradient is highest.
Ataei-Dadavi et al. did experiments[7] on a side heated empty cavity and found a power law corresponding to the results which is plotted in fig4.1. As can be seen the empty cavity simulations correspond well to this power law.

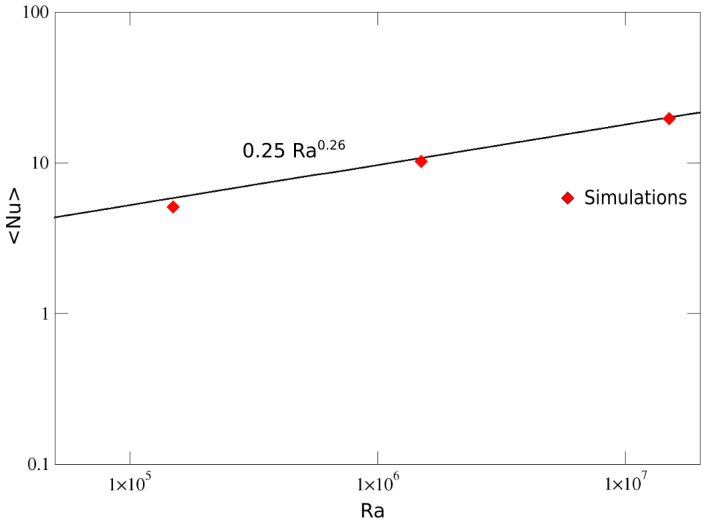

Figure 4.1: Nu number against Ra. The line represents the power law Rounaghi [26] found by doing experiments. The three diamonds are simulations of the only fluid case to validate the mesh.

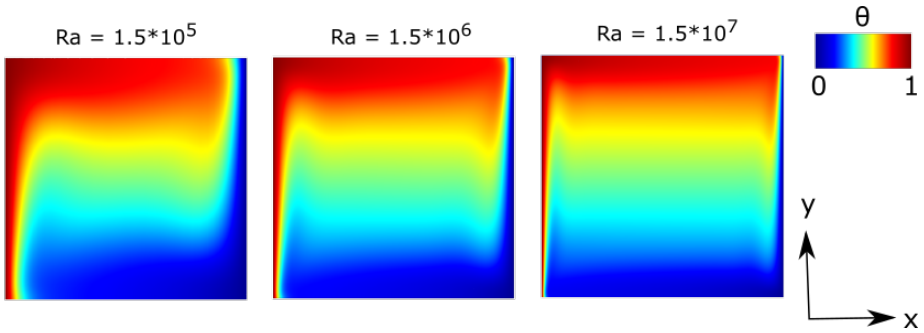

Figure 4.2: Temperature contours at Ra 10^5, 10^6 and 10^7 of the only fluid case.

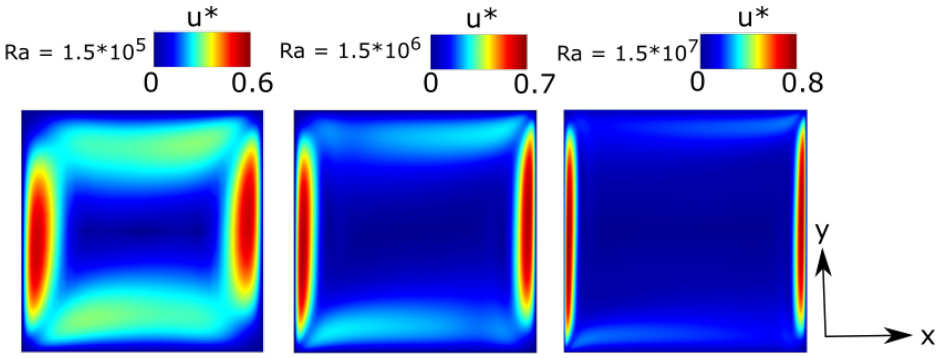

Figure 4.3: Velocity contours at Ra 10^5, 10^6 and 10^7 of the only fluid case.

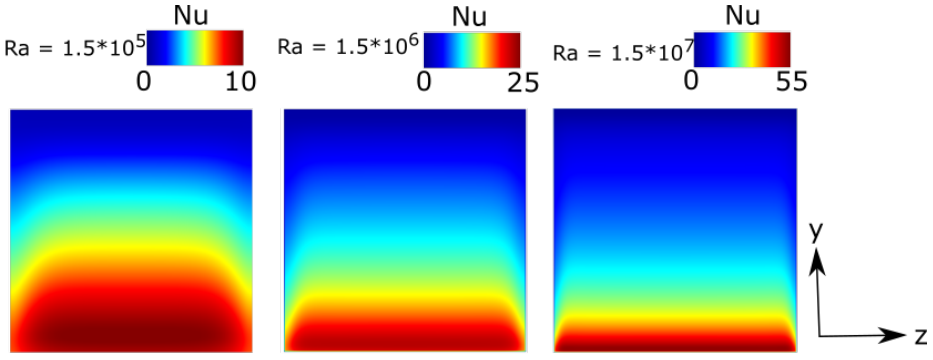

Figure 4.4: Velocity contours at Ra 10^5, 10^6 and 10^7 of the only fluid case.

5

Objects unattached to the wall

Simulations are done at Ra = $10^5, 10^6$ and 10^7 in a cavity filled half with aluminum objects ($\lambda^* = \frac{\lambda_{Al}}{\lambda_f} = 337.33$) and half with wooden objects ($\lambda^* = \frac{\lambda_W}{\lambda_{fluid}} = 0.29$). The objects are all the same distance from each other which is also the distance from the object to the wall. Four different configurations are studied from here on called Case A to D and can be seen in figure 1.2. First the temperature contours and boundary layer are discussed after which the velocity fields and Nu contours are discussed. Finally the thermal disequilibrium will be discussed.

5.1. Temperature field

Figure 5.1 shows the temperature contours of the simulations done of the only fluid case and the four cases with objects, all done at Ra = $10^5, 10^6, 10^7$. The contours are taken at two cross-sections. The first cross-section is through the middle at $z/W = 0.5$ and shows only fluid and no objects. The second cross-section is at $z/W = 0.4$ so that the temperature contours through the objects can also be observed.

Temperature field at Ra = 10^5

Figure 5.1a show the temperature contours at Ra = 10^5. The only fluid case shows horizontal temperature gradient at the hot and cold wall and a vertical temperature gradient in the middle of the cavity. The cases A to D show more diagonal temperature gradient with in the middle linearly temperature behaviour, indicating conduction dominated regime. This is also confirmed when looking at the velocity and Nu in sections 5.3 and 5.4.

The big question is: 'do the objects influence the heat transfer?' The temperature contours can give us two hints about how the objects interact with the fluid. First, when looking at the temperature contours of the objects along the $z/L = 0.4$ plane the wooden objects show a linear temperature gradient between the cold side to the warm side. Which side of the object is cold or warm and how big this temperature gradient is depends on the surrounding fluid. The aluminum objects are however isothermal, with the temperature that corresponds to the average temperature of its surrounding fluid.

Secondly, when looking at plane $z/L = 0.5$ isothermal regions can be observed in the fluid. These regions correspond to fluid surrounded by two aluminum objects. As the fluid has a very low conductivity this isothermal behaviour can only be explained by the transfer of heat between the fluid and the aluminum objects.

These two aspects results in Case A, who has only conducting objects at the wall, having a more isothermal hot region at the wall that extends until after the first column of objects while Case B has a temperature gradient close to the wall across the first object. Case C shows isothermal behavior at the first and fourth object from the bottom while having a temperature gradient at the second and third object. Case D starts with a temperature gradient at the wall and continues with an isothermal region at the second and third object while finishing again with a temperature gradient at the fourth object.

Temperature field at Ra = 10^6

In figure 5.1b the temperature contours of the two cross-sections $z/L = 0.4$ and $z/L = 0.5$ are shown at a Ra = 10^6. The only fluid case has the same vertical and horizontal temperature profile can be seen as at Ra =

10^5, but this time the temperature gradient at the walls is bigger. This results in a smaller boundary layer. The plume created at the wall is also bigger which is the result of the higher vertical momentum by the fluid created by the stronger buoyancy force.
When comparing the left bottom corner (the start of the boundary layer) of the temperature contours of Case A to D they show a similar temperature gradient. This is different than at Ra = 10^5 where the boundary layer was different depending on the configuration of the objects. But with Ra = 10^6, the configuration doesn't matter. This is because the natural convection is strong enough to circulate cold water close enough to the wall so that the boundary layer is entirely in front of the first column of objects. The same two influences between fluid and objects can be seen here as described in the previous section: The wooden objects have a temperature gradient while the aluminum objects have an isothermal temperature. And the fluid in between two conductive objects have the same temperature as the conductive objects surrounding them because of heat transfer between the object and the fluid. However because the boundary region is now in front of the first column of the thermal boundary layer of all cases look similar.

Temperature field at Ra = 10^7

In figure 5.1c the temperature contours at a Rayleigh number 10^7 can be seen. The only fluid case has an even smaller boundary layer and a higher plume than at Ra = 10^6. When looking at plane $z/W = 0.5$, a plume can be seen in all the temperature contours at $z/W = 0.5$. The flow is now strong enough to create a plume even if there are objects in it.

5.2. Boundary Layer

Figure 5.2a and 5.2b show the boundary layer (BL) thickness measured at $y/H = 0.1$ and $y/H = 0.5$ respectively. Thickness δ_{99} is defined as the x-coordinate where the temperature becomes 99% of the mean temperature when measuring the temperature along a line from $x/L = 0$ to $x/L = 1$ at $z/L = 0.5$ and at either $y/H = 0.1$ (which is at the bottom) or at 0.5 (which is at the center).

Boundary layer at Ra = 10^5

The only fluid case has a δ_{99} at $y/H = 0.1$ of 0.06 and at $y/H = 0.5$ of 0.13 showing that there is a much smaller boundary layer at the bottom than at the middle. When looking at the four cases with objects all of them have a δ_{99} of 0.5 at $y/H = 0.5$. This is because there is not enough natural convection to create a thermal plume in the cases with objects and thus the mean temperature will be only met in the center of the cavity.
All four cases have at $y/H = 0.1$ larger δ_{99} than the only fluid case. This is because there is less natural convection and thus there is a broader boundary layer. Case A and C, which have conductive objects at the wall, have a similar δ_{99} at 0.25. While Case B and D, who have insulating objects at this place have a δ_{99} of 0.17. Conductive objects thus thicken the boundary layer. This is because conductive objects improve the heat transfer from the walls as will become clear in section 5.4.

Boundary layer at Ra = 10^6

The only fluid case has a value of δ_{99} of 0.07 at $y/H = 0.5$, this is two times smaller than the δ_{99} of 0.13 for Ra = 10^5 only fluid case, showing that a higher Ra number reduces the boundary layer thickness significantly. At $y/H = 0.1$ the values of δ_{99} of all four cases are very similar to the only fluid case at 0.026 and no effect of the objects can be seen. This is different than in the Ra = 10^5 where conductive objects extended the boundary layer and insulating objects reduced the boundary layer. The reason for this is that the boundary layer at $y/H = 0.1$ is before the first column of objects situated at $x/L = 0.065$. There is enough natural convection for the cold fluid to surpass the column of objects close to the wall. This means that the wall can transfer heat to the fluid and natural convection can take place without interference of the first column of objects.

Boundary layer at Ra = 10^7

The δ_{99} of the only fluid case has again decreased with a factor 2 compared to Ra = 10^6. At $y/H = 0.5$ it is 0.04. Different from the Ra = $10^5, 10^6$ at Ra = 10^7 there is a plume at $y/H = 0.5$. This causes the δ_{99} to be closer to the wall at 0.043. This is only marginally larger than that of the only fluid case. At $y/H = 0.1$ the values of δ_{99} of all cases are instead marginally smaller at 0.014 compared to the only fluid case at 0.015. This is because the objects push the flow more to the wall.

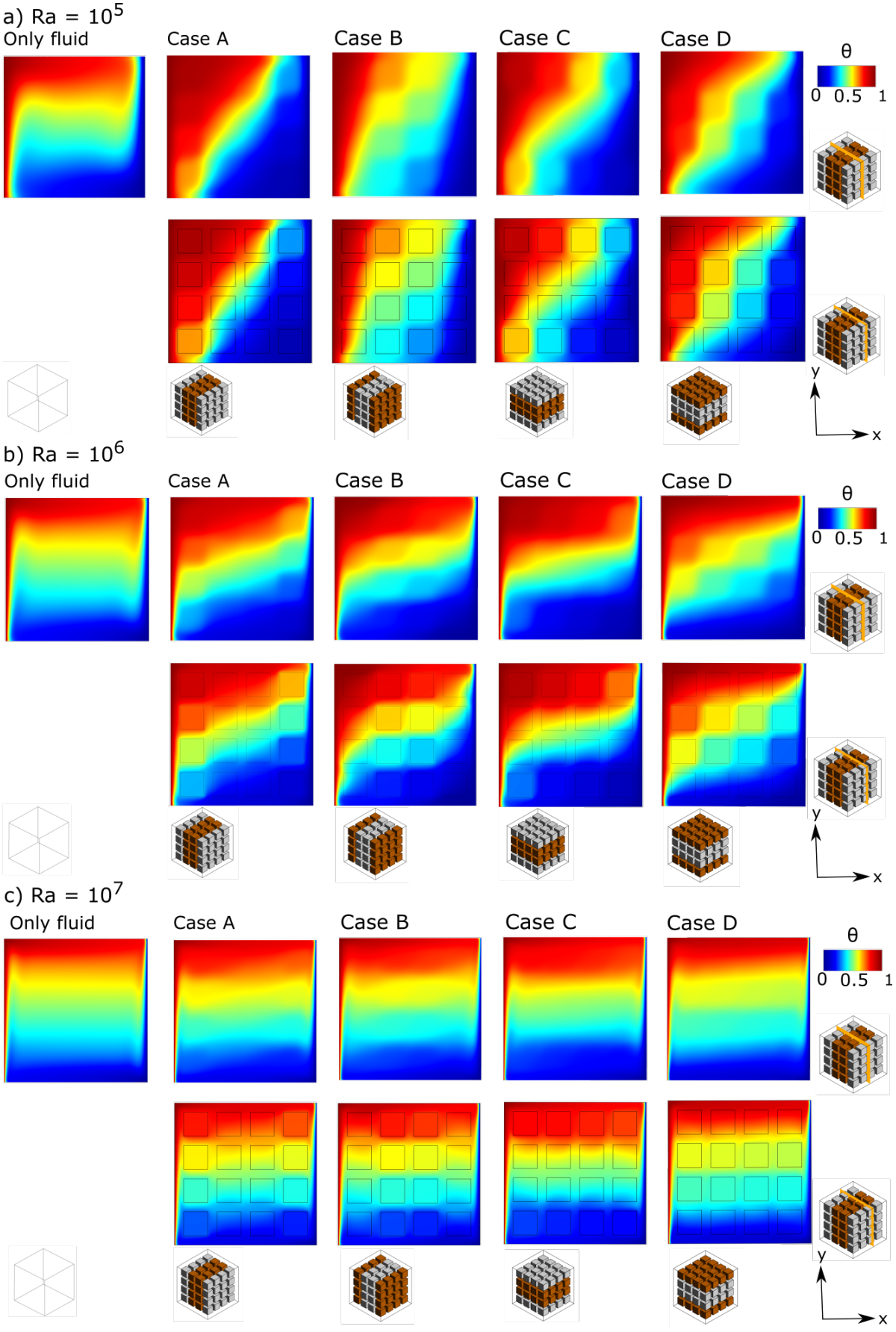

Figure 5.1: Temperature contours when objects are not attached to the walls at a) Ra = 10^5, b) Ra = 10^6 and c) Ra = 10^7. The contours are taken at two planes, at $z/W = 0.5$ and $z/W = 0.4$.

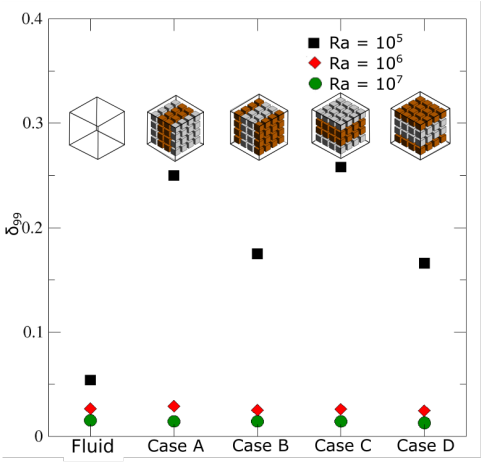

(a) The boundary layer thickness when objects are not attached to the wall at $y/H = 0.1$

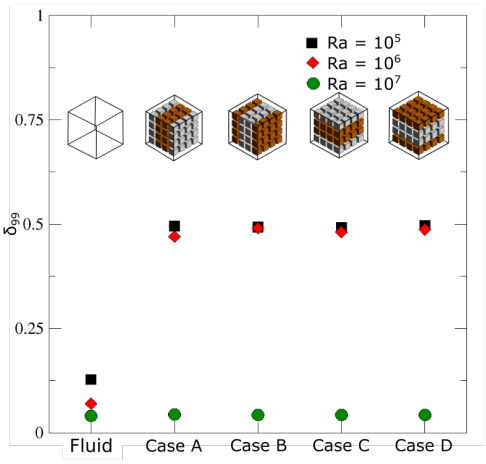

(b) The boundary layer thickness when objects are not attached to the wall at $y/H = 0.5$

5.3. Velocity field

Similar cross-sections that are used for the temperature contours are also used for the velocity fields in figure 5.3. The velocity is normalized by[36]:

$$u^* = \frac{\sqrt{u^2 + v^2 + z^2}L}{Ra^{3/7}\alpha} \tag{5.1}$$

Figure 5.5 shows the RMS of the volume averaged Re of the whole cavity for Case A to D. The Re is calculated as followed:

$$U_i = \sqrt{u^2 + v^2 + z^2} \tag{5.2}$$

$$U_{RMS} = \sqrt{\frac{\sum_{i=1}^{N} U_i^2 VOL_i}{\sum_{i=1}^{N} VOL_i}} \tag{5.3}$$

The square velocity at each location in the fluid domain (U_i) is multiplied with the volume of the cell of that location(VOL_i) and summed up. This is divided by the total volume of the fluid domain and the square root is taken. The Re number is then divided by Re_0, the Re of the only fluid case to make comparison possible.

Velocity fields at Ra = 10^5

Figure 5.3a shows the velocity fields at Ra = 10^5. When comparing the only fluid case with the Case A to D it can be seen that u^*_{max} of the only fluid case reaches 0.6, while u^*_{max} of the cases with objects only reaches 0.3. This is because the four cases consist 30% out of solid objects that are blocking the flow. The fluid shows preference for flowing in the channels that emerge between four objects because the fluid has more degrees of freedom there.

A lot of difference in flow behaviour can be seen between the four cases when looking at the plane $z/L = 0.5$. When comparing Case A and B, two major differences can be seen. First the flow in the boundary layer of Case B is larger compared to Case A. This can be explained by the fact that in Case A the temperature gradient is smaller due to aluminum objects conducting heat from the boundary layer towards the center of the cavity. This can be the seen in the temperature contours in figure 5.1a. A smaller temperature gradient will create a smaller buoyancy force and thus a lower velocity. While Case B has an insulating objects at the wall creating a big temperature gradient and bigger buoyancy force at the wall.

Secondly, when looking at the space in between the objects close to the hot and cold wall a higher velocity can be seen in Case A than in Case B. This is because the conductive object transfer heat from the hot wall side to the sides of the object, heating the fluid in between the objects and causing a buoyancy force at the objects. This is illustrated in figure 5.4.

Case C shows a strong velocity at the boundary at the second and third object at the wall. At these two places the case has insulating objects, thus showing again that insulating objects increase boundary layer flow. Although the boundary layer flow is not as strong as in Case B, probably because Case C has only two insulating objects at the wall.
Case D shows low velocity in between the bottom objects and a higher velocity in between the middle objects. Showing again that conducting objects improve flow in between them.
When looking at the relative Re in figure 5.5 the Re doesn't differ a lot. Case A shows a slightly higher Re. The conductive objects at the wall increase the buoyancy force between the objects while decreasing the buoyancy at the wall. The slightly higher Re shows that the first effect dominates, but barely.

Velocity fields at Ra = 10^6

The same cross-sections can be seen for the velocity fields in figure 5.3b. The only fluid case shows the same circulation. Only now with a thinner momentum boundary layer and higher velocity magnitude. Unlike the velocity fields of Ra = 10^5 all four cases show the same profile: A center that is almost stagnant and a high flow at the hot and cold walls. The reason for no change is because as explained in the previous section the boundary layer doesn't extend to the first column of objects. Natural convection takes place in the boundary layer without being influenced by the first column of objects and as almost all momentum is created at the boundary layer this results in very similar velocity fields. When looking at the Reynolds number seen in figure 5.5 the numbers are close to each other. Case A and C show a slightly lower Re than Case B and D. This is caused by the conducting objects at the bottom who decrease the temperature gradient slightly and thus reduce the natural convection. But this effect only causes a 5% difference in Re.

Velocity fields at Ra = 10^7

The velocity fields for Ra = 10^7 can be seen in figure 5.3c. The only fluid profile shows a very thin momentum boundary layer. This small boundary layer is where most of the velocity is and when looking at the four cases with objects in them it can be seen that the whole momentum boundary layer fits between wall and the first object. This explains why there is so little effect seen of the objects when looked at the temperature contours and the temperature boundary layer. When looking at the Re numbers in figure 5.5 all cases have a similar Re of 1.18. At first it can look surprising that the cases with objects in them have a higher value than 1 because the objects always obstruct some flow. The reason that Re/Re_0 is higher than 1 is because in its calculation only the fluid domain is considered because there is no flow possible in the objects. The only fluid case consist out of 60% of almost stagnant region ($U < 0.1U_{max}$). This stagnant center brings the averaged Re down during averaging. The cases with objects in them consist 30% of which almost all of it is inside the stagnant center. The stagnant center of Case A to D thus doesn't reduce the average value of Re as much as the only fluid case resulting in a value above 1 when dividing by the Re of the only fluid case.

5.4. Heat transfer

The Nusselt number is a good way to see if the heat transfer is conduction dominated or convection dominated and is also a good way to normalize the heat flux. In figure 5.6 the Nu at the hot wall can be seen. This Nu number is calculated as:

$$Nu = \frac{q_{wall} \cdot L}{\lambda(T_{wall} - T_{mean})} \tag{5.4}$$

As can be seen in the formula the only varying parameter is the heat flux q_{wall}, meaning that the Nu number tells us how much heat is extracted from the wall. High Nu means that a lot of heat is extracted from the wall while low Nu means that there is little heat extracted from the wall. Figure 5.7 shows the surface averaged nusselt number (<Nu>) of the hot wall. The <Nu> is normalized by dividing it by $<Nu>_0$, the <Nu> from the only fluid case.

Heat transfer at Ra = 10^5

Figure 5.6a shows the Nu contours of Ra = 10^5. When looking at the only fluid case the bottom of the hot wall shows a high Nu. This is also the place where the temperature gradient is the highest as can be seen in the temperature contours of figure 5.1a. The high temperature gradient causes a high heat transfer and a high buoyancy force which causes high convection. The Nu decreases with increasing y/H at the wall. This

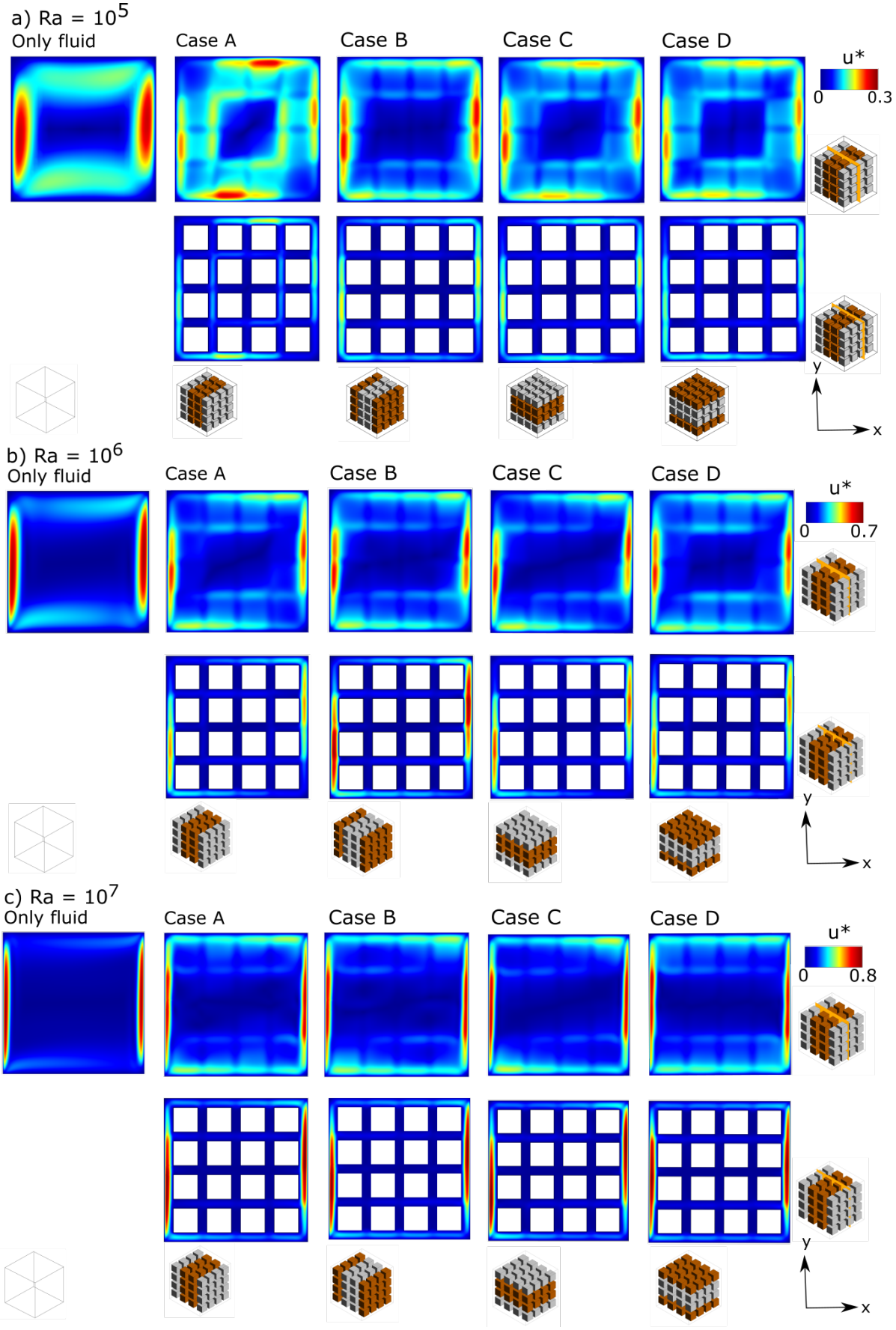

Figure 5.3: Contours of non-dimensional velocity magnitude when objects are not attached to the walls at a) Ra = 10^5, b) Ra = 10^6 and c) Ra = 10^7. The contours are taken at two planes, at $z/W = 0.5$ and $z/W = 0.4$.

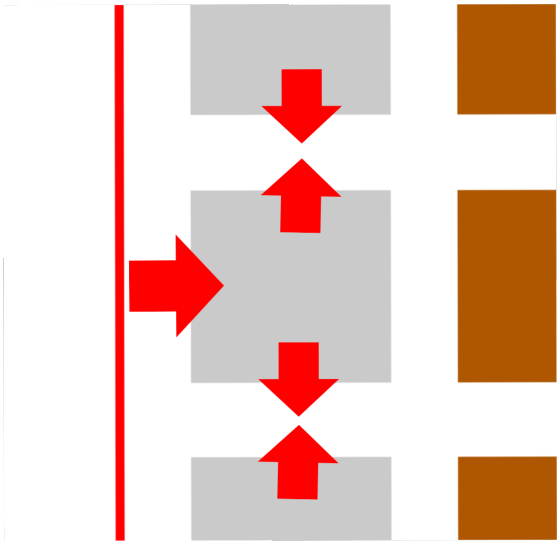

Figure 5.4: Schematic view how the conductive objects heat the fluid from the side. The heat is transferred from the wall through the conductive objects to the sides.

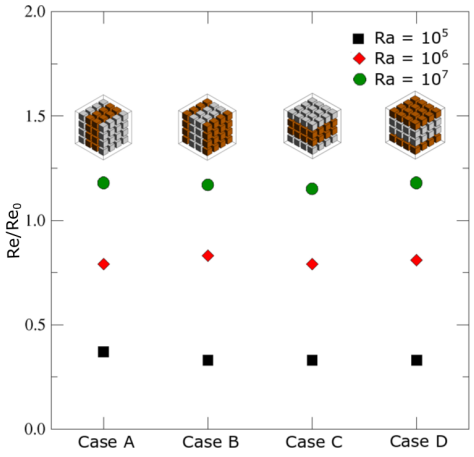

Figure 5.5: The Volume averaged RMS of Re when objects don't touch the walls. The Re is normalized by dividing to the Re of the only fluid case.

is because the fluid is heated up when it flows along the wall. The temperature difference decreases and so does the heat transfer from the wall to the fluid.
The four cases with objects show that objects in the vicinity of the wall influence the heat transfer at the wall. Case A, with only conductive objects, show high Nu at the places at the wall that have object in their vicinity. Case B, with only insulating objects, shows on the other hand a lower Nu at these places. Case C and D have conductive and insulating objects and it can be seen that at the places at the wall close to conductive objects the Nu increases while at the places at the wall where there are insulating objects the Nu decreases. The reason Nu increases when in the vicinity of conductive objects and decreases in the vicinity of insulating objects is because heat always seeks the path of least resistance. Conductive objects decrease the thermal resistance of the boundary layer at these places at the wall while the insulating objects increase the thermal resistance. The places on the wall with least thermal resistance will extract most heat while places on the wall with large thermal resistance will have a small heat flux.
When looking at figure 5.7 it can be seen that all values of the cases are below 1. This means that there is less heat flux extracted from the wall than the only fluid case. This is because the objects obstruct flow, creating less temperature gradient at the wall and thus a lower heat flux.
Of all the cases Case B has the smallest <Nu> (<Nu>/<Nu>$_0$ of 0.31). This is because Case B has insulating objects at the wall that decrease the Nu. One would expect a higher <Nu> for Case A which has only conductive objects than Case C and D where only half of the objects are conductive and the other half is insulating. But as 5.7 shows the <Nu>/<Nu>$_0$ for all three cases are similar around 0.45 with the <Nu>/<Nu>$_0$ of Case A only slightly higher at 0.47. This might be explained by the fact that conductive objects also dampen natural convection. Conductive objects decrease the thermal gradient and thus the buoyancy force. This thermal gradient is still present in Case C and D who have also insulating objects in them. Natural convection corresponds with a high Nu at the bottom of the wall which can be seen in Case C and D. In Case A this Nu at the bottom is a bit lower than the other cases, indicating lower natural convection.

Heat transfer at Ra = 10^6

In figure 5.6b the Nusselt contours at Ra = 10^6 can be seen. Unlike the Nu contours of Ra = 10^5 the contours for Ra = 10^6 don't show a lot of difference. The Nu contours show a wavy character. This is caused by the objects close to the wall. They reduce the flow and thus reduce the amount of convection. The peaks shown in the Nu contours corresponds to the slits between the objects in the z-direction where it is easier for fluid to flow, while the valleys corresponds to where the objects are in the z-direction. It can be seen that the wavy character is stronger in Case B and D than in Case A and C. This is because the bottom column of objects in Case B and D are made of insulating objects. The heat flux at the places at the wall that face the objects is both reduced due to the increased resistance of the insulating objects and because the flow is reduced be-

cause there is an object in place. Case A and C have on the other hand conductive objects at the bottom. The high conductivity of the objects enhance the Nu at the wall, although this effect is very small, while the object blocks the flow and decrease the Nu at the wall. These two effects oppose each other and thus decrease the wavy character.
When looking at Figure 5.7 it can be seen that the <Nu>/<Nu>$_0$ at the hot wall off all the cases are around 0.75. This is higher than the case of Ra = 10^5 meaning that the flow is less obstructed by the flow. This is because most flow is now in between the wall and the outer objects. This also explains why there is almost no difference between the <Nu> of all the cases.

Heat transfer at Ra = 10^7

The Nu contours at the hot wall can be seen in figure 5.6c. The Nu has only a high value at the very bottom of the cavity. The wavy character seen in Ra = 10^6 is much smaller. There are still some small peaks in between the objects but overall it looks more like the only fluid case. When looked at the graph in 5.7 it can be seen that the <Nu>/<Nu>$_0$ is almost 1. There is almost as much heat transfer as in the only fluid case because all objects are in the stagnant center and don't influence the heat transfer in the cavity anymore.

5.5. Thermal disequilibrium

A useful term that indicates interaction between objects and fluid is the thermal disequilibrium (DT) [37]. The thermal disequilibrium is measured by dividing the cavity into units in such a way that each unit has an object at his center. Then the ratio is calculated of the average temperature of solid and the fluid through:

$$|DT|\% = |1 - \frac{< T_s >}{< T_f >}| \cdot 100\% \tag{5.5}$$

In the equation $< T_s >$ and $< T_f >$ are the volume averaged temperature of the solid and fluid respectively.

Thermal disequilibrium at Ra = 10^5

Figure 5.8 shows the DT of four objects at the hot wall where the most action happens. The higher the temperature difference is across a single unit, the higher the DT is. This can be seen as all 4 cases have low temperature difference at the top unit and all cases show low DT in unit 3 and 4. Units with conductive objects in them also show low DT because the conductive objects tend to be isothermal and exchange heat with the surrounding fluid and thus making the surrounding fluid also more isothermal. Insulating objects at the bottom however have a large temperature and thus a high DT.
Case A (the black squares) shows a low DT throughout all units. Case A only has conducting objects along the wall which have no trouble transferring heat from and to the fluid. This results in a low DT across all units.
Case B (red diamonds) has only insulating objects who have bad heat transport between object and fluid. This can be seen in the graph where they have the highest DT of all cases. The DT of Case 2 at Unit 1 is the highest as the cold water arrives there at the hot wall and thus the highest temperature difference exist across the unit. The higher the unit is along the wall the more the water is heated up and the less the temperature difference is across the unit, which results in a lower DT.
Case C (green dots) starts with a conducting object in Unit 1 and thus has low DT there. Unit 2 is insulating and thus has lower DT. The DT in Unit 3 drops again as the temperature difference across the unit is lower.
Case D (purple triangles) has an insulating object at the bottom in Unit 1. This unit has a very high DT. The rest of the units have very low DT as Unit 2 and 3 contain conductive objects and Unit 4 is at the top of the cavity where the temperature gradient is very low.

Thermal disequilibrium at Ra = 10^6

Figure 5.9 shows the DT of the four cases at Ra = 10^6. The overall DT in the units is approximately twice as strong as in the cases of Ra = 10^5. The same behaviour is shown again. Units with conductive objects in them show low DT while units with insulating objects in them show high DT. Also lower objects show in general higher DT. There is however an exception at Unit 1 in Case 4 is low while it has an insulating object in it. It is uncertain why this is.

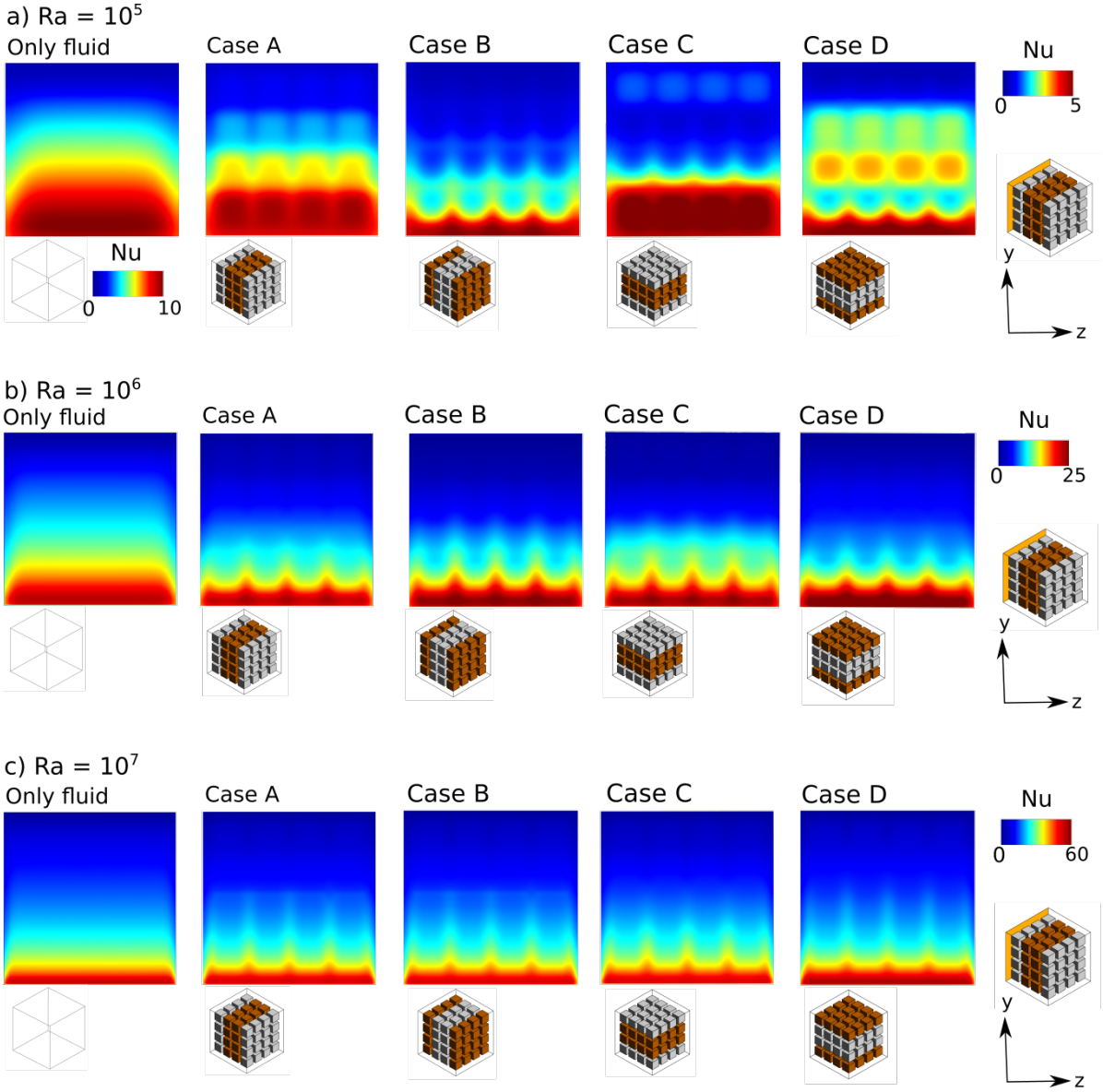

Figure 5.6: Contours of the local Nu at the hot wall when objects are not attached to the walls at a) Ra = 10^5, b) Ra = 10^6 and c) Ra = 10^7.

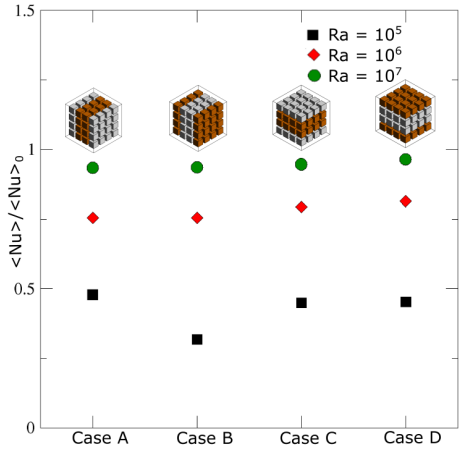

Figure 5.7: Average Nusselt number at the hot wall when objects are not attached to the wall. The <Nu> is normalized by dividing over the <Nu> of the only fluid case.

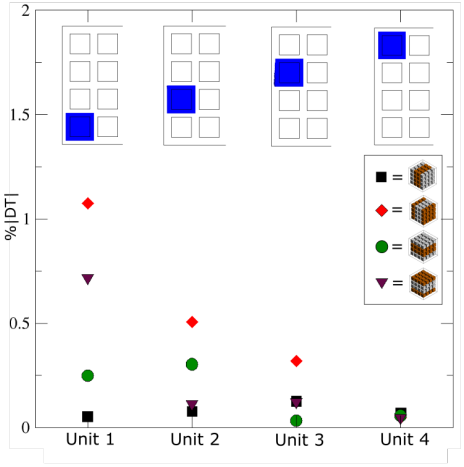

Figure 5.8: Thermal disequilibrium between objects and the fluid when the objects are not attached the wall at Ra = 10^5.

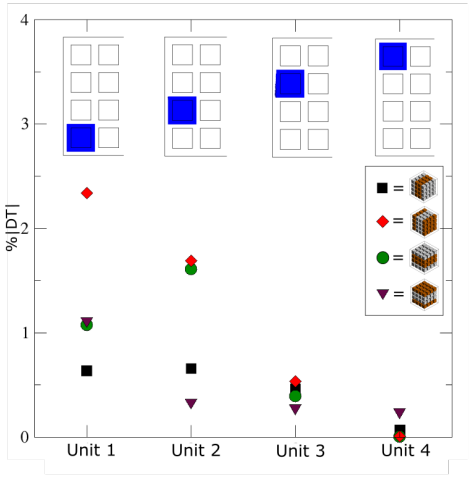

Figure 5.9: Thermal disequilibrium between objects and the fluid when the objects are not attached the wall at Ra = 10^6.

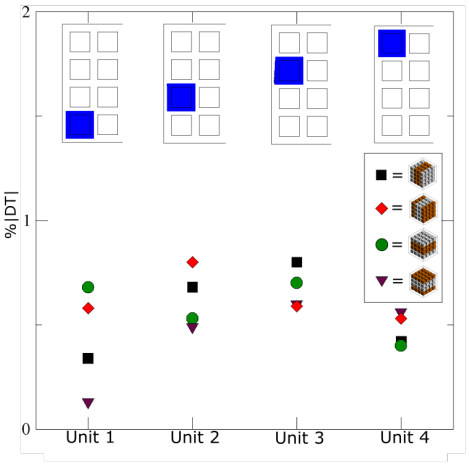

Figure 5.10: Thermal disequilibrium between objects and the fluid when the objects are not attached the wall at Ra = 10^7.

Thermal disequilibrium at Ra = 10^7

Figure 5.10 shows the DT at Ra = 10^7. The overall DT is below 1% and shows very different behaviour than at Ra of 10^5 and 10^6. The DT doesn't decrease as y increases anymore. There is a slightly higher DT found at Unit 2 and 3. It also doesn't make a difference anymore if the unit contains a conducting object or a insulating object. The reason for these two changes is the higher circulation in the cavity at Ra = 10^7. This causes the flow to be closer to the walls and less in the units. Less flow in the units corresponds to less strong DT. The temperature gradient is now big at the almost the whole length in cavity due to high circulation, thus causing also relative high DT in units 2 and 3 compared to unit 1. As the flow is close to the wall the objects hardly exchange heat anymore with the fluid. Thus there is no difference in DT anymore between the conducting and insulating objects.

5.6. Summary and conclusion

Simulations have been done at Ra = $10^5, 10^6, 10^7$ on four cases with different configurations of conductive and insulating blocks. At Ra = 10^5 conductive blocks show an increase in heat transfer at the wall and flow in between the objects while insulating blocks show decrease of heat transfer at the wall and more flow at the walls. At Ra = $10^5, 10^6$ the flow is to close to the wall for the objects to influence the heat transfer or the flow and hardly any differences between the cases can be seen.

6

Objects attached to the wall

The same configurations as previous chapter are studied but now the objects in the vicinity of the wall are attached to the wall. Heat can directly flow into the objects from the wall. First the temperature contours are discussed. Then the boundary layer, velocity field and Nu contour and lastly the thermal disequilibrium.

6.1. Temperature field

Figure 6.1 shows the temperature contours of Case A to D at Ra = $10^5, 10^6$ and 10^7. The temperature contour are shown at two planes, at $z/L = 0.5$ and $z/L = 0.4$. In the case were the objects didn't touch the wall all objects were surrounded by the fluid. Through the wooden objects had a temperature gradient from the hot side of the fluid to the cold side while the conducting objects were isothermal with a temperature average of that of the surrounding fluid. The middle columns of objects are still surrounded by fluid and still have this behavior. But the outer columns touch directly the walls and heat can directly conduct into the objects. The wooden objects, who are insulators, conduct very little heat from the wall and create a temperature gradient between the wall and the fluid. The aluminum objects however are very conducting and absorb a lot of heat from the wall and are the same temperature as the wall. They can basically be seen as extensions of the wall.

Temperature field at Ra = 10^5

Figure 6.1a shows the Temperature contours at Ra = 10^5. Case A only has aluminum objects attached to the walls. When looking in figure 6.1a at the $z/L = 0.4$ plane that cut through the objects it can be seen that the aluminum has the same temperature as the walls they are attached to. This is because aluminum has a much higher conductivity as the fluid and can conduct directly heat into the objects. When comparing the $z/L = 0.4$ and the $z/L = 0.5$ plane most of the temperature profile looks the same with isothermal regions in between the objects. Just like the case where the objects were not attached, the aluminum objects transfer heat to its surrounding fluid.
Case B has only insulating objects at the walls. The objects have a high thermal resistance so the heat from the wall only wants to transfer directly from the wall into the fluid. The objects attached to the walls however block most of the wall and only little wall is left for heat to be transferred to the fluid. There is not a lot of heat transferred to the fluid and thus little buoyancy force. This results in a conduction dominated regime which look like the vertical temperature profile seen in Case B.
Case C and D have both insulating and conducting objects attached to the wall and when looking at their temperature contours it can be seen that the position of these objects matter. Case C has conducting objects at the top and bottom and insulating objects in the middle. When looking at plane $z/L = 0.4$ the lowest and highest object at the hot wall can be seen as extension of the wall with the objects taking the same temperature as the wall. Because the lowest object is the same temperature as the wall it extends the boundary layer to beyond the first row of objects. But there is also a small retraction of the hot temperature across the middle objects because they are insulating and create a temperature gradient.
In Case D the objects at the top and bottom are insulating while the objects in the middle are conducting. When looking at plane $z/L = 0.4$ it can be seen that it has a smaller boundary layer at the bottom object than Case A and C have. When the cold fluid reaches the object second to the bottom, which is conducting, the boundary layer is suddenly extended past the first column of objects.

Temperature field at Ra = 10^6

Figure 6.1b shows the temperature contours at a Ra = 10^6. The contours look similar to the cases at Ra = 10^5 discussed in the previous section. Although, now the natural convection is strong enough to get hot fluid to the top of the cavity and cold fluid to the bottom. This causes some differences in the four cases.
At Case A, a small difference between the two temperature contours $z/L = 0.4$ and $z/L = 0.5$ can be seen at the object in the bottom left corner. While plane $z/L = 0.4$ show a completely isothermal temperature profile for the bottom object located attached to the wall, at plane $z/L = 0.5$ the fluid in between the objects is not completely isothermal. This is remarkable because as discussed in section 5.1 aluminum objects are very good at transferring heat to and from the fluid. But because there is a large buoyancy force created between the objects they are not able to heat the liquid between them fast enough to make the region isothermal. Case B shows now mostly horizontal profile in the center of the cavity. This is because there is enough natural convection to convect heat at the top of the cavity, where the conductive objects in the center can increase the heat transfer from left to right. Case C and D look very similar to their counterparts at Ra = 10^5, but with a stronger circulation the top has a higher temperature.

Temperature field at Ra = 10^7

Figure 6.1c shows the temperature contours at a Ra = 10^7. The first thing noticeable is that the $z/W = 0.5$ and the $z/W = 0.4$ planes are very different from each other. The contours at plane $z/W = 0.5$ all have a very small boundary layers which is comparable to the only fluid case. In the $z/W = 0.4$ plane however the conductive objects extend the boundary layer to the edge of the object. This result in very different thermal boundary layer for the two different planes. The reason for this is that at Ra = 10^7 the flow is strong enough for the cold water to reach the hot wall.
This can be seen clearest in Case A. Case A has only conducting objects and in all the previous Cases A with lower Ra and not attached to the wall the conducting objects were able to heat the fluid in between them in time to get an isothermal region in plane $z/W = 0.5$. But now the flow is so fast that the objects don't have time to heat the fluid passing by.
When looking at plane $z/W = 0.5$ of Case A a second peak in the temperature contours can be seen after the first peak. This corresponds to a second boundary layer caused by conducting objects. The aluminum objects conduct heat from the wall to the edge and transfer it to the water. Thus there is heat transferred from the wall to the fluid and from the objects to the fluid there are two thermal boundary layers created.
When looking at Case B at plane $z/W = 0.5$ a very smooth temperature profile can be seen with vertical profile close to the wall and horizontal in the center. Case B doesn't have conducting objects at the wall to create a second boundary layer so only one thin boundary layer can be seen close to the wall. The objects do however block the flow enough to prevent a plume in the boundary layer. In plane $z/W = 0.4$ there is a larger thermal boundary layer than in plane $z/W = 0.5$. This is because the insulating objects create a very linear temperature gradient across the object. This is unlike the boundary layer which is convected close to the wall.
Plane $z/W = 0.4$ of Case C is very similar to that of Ra = 10^6. But plane $z/W = 0.5$ shows the same behaviour as the other cases with the thermal boundary layer close to the wall. The lower and top object are conducting transfer heat to the edge and plumes can be seen at these places. When looking at Case D at plane $z/W = 0.5$ those peaks can be seen at the second and third object, as they are the conducting objects of this case.

6.2. Boundary layer

Figure 6.2a and 6.2b shows the δ_{99} of the objects attached to the wall at $y/H = 0.5$ and $y/H = 0.1$ just like in the cases where the objects didn't touch the wall. For Ra = 10^6 and 10^7 the δ_{99} is measured both at $z/W = 0.5$ and $z/W = 0.4$ because they start to differ at these Ra.

Boundary layer at Ra = 10^5

Just like the cases with objects not touching the wall the δ_{99} at $y/H = 0.5$ is 0.5 as there is again no thermal plume. Case A, B and C all show δ_{99} around 0.23 while Case D has a δ_{99} of 0.15. Case A and C have conductive objects at the bottom that conduct heat and extend the boundary layer to after the first layer. This also happens with the Case A and C when the objects didn't touch the wall but because the objects are now closer to the wall the δ_{99} is smaller(a δ_{99} of 0.23 compared to a δ_{99} of 0.26).
Case B insulating objects creates a temperature gradient at the wall but does not have a flow that push cold fluid to the wall to create a steep temperature gradient like what happens in the only fluid case. So the δ_{99} still

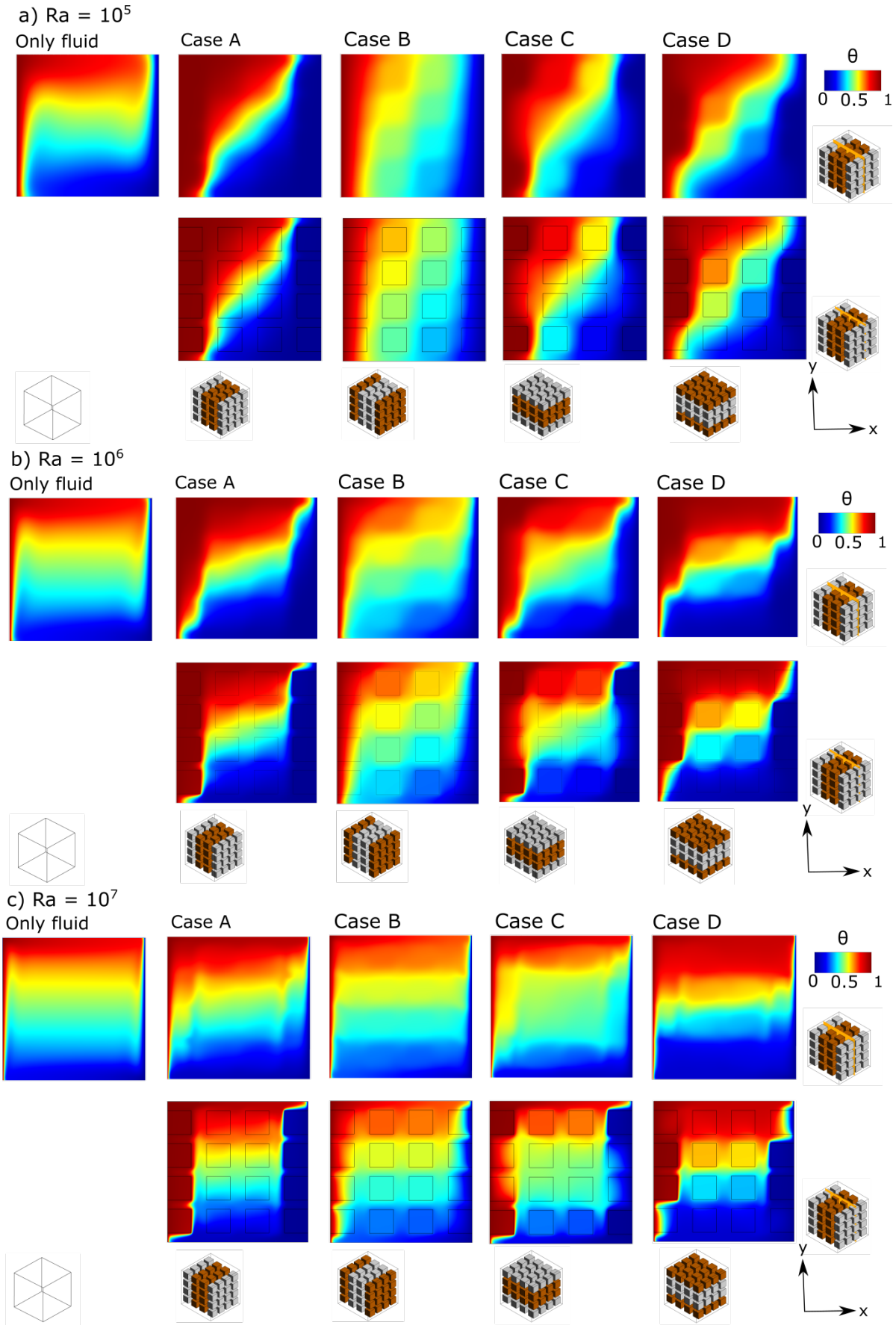

Figure 6.1: Temperature contours when objects are attached to the walls at a) Ra = 10^5, b) Ra = 10^6 and c) Ra = 10^7. The contours are taken at two planes, at $z/W = 0.5$ and $z/W = 0.4$.

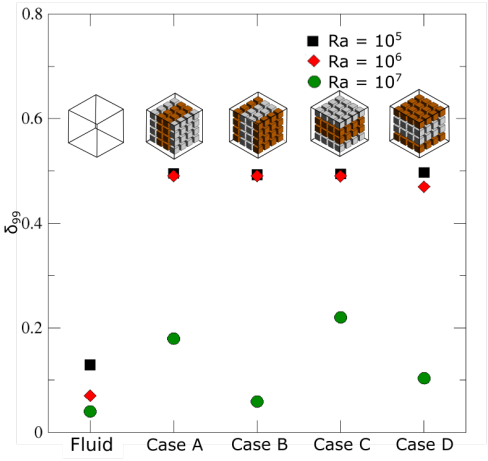

(a) The boundary layer thickness when objects are attached to the wall at $y/H = 0.5$

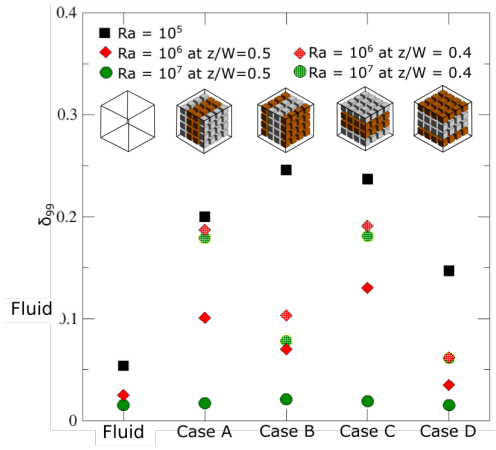

(b) The boundary layer thickness when objects are attached to the wall at $y/H = 0.1$

extends to after the first object. Because there is less flow in Case B with the objects attached to the wall than Case B with the objects not attaching the wall, δ_{99} is larger this time compared to the case with the objects not attached to the wall(a δ_{99} of 0.25 compared to a δ_{99} of 0.17).
Case D has an insulating object at the bottom that creates a temperature gradient and a flow to reduce the temperature gradient even further. It has the smallest δ_{99} of 0.15 of all the cases with objects attached to the wall. It has a stronger flow than Case D without the objects touching the wall and also a smaller boundary layer (a δ_{99} of 0.15 against a δ_{99} of 0.17).

Boundary layer at Ra = 10^6

Similar to the cases of objects not touching the walls and the Ra = 10^5 the δ_{99} is 0.5 at $y/L = 0.5$. At $y/L = 0.1$ has different values depending on the plane. At $z/W = 0.4$ the δ_{99} of Case A and C which have conducting objects at the bottom is extended to after the object at 0.19. It is less than their Ra = 10^5 counterpart as the flow is stronger and boundary layer at the edge of the object is smaller. When looking at $z/W = 0.5$ the values of δ_{99} are even smaller, 0.1 and 0.13 for Case A and C respectively. The stronger flow pushes water in between the conducting objects creating a smaller boundary layer there.
Case B and D have insulating objects at the bottom. The δ_{99} at $z/W = 0.4$ and $z/W = 0.5$ are relatively close to each other. Case D has the lowest δ_{99} of all cases because it has insulating objects at the wall that don't extend the boundary layer and flow in it that pushes the boundary to the wall.

Boundary layer at Ra = 10^7

The flow of at Ra = 10^7 is so strong in all cases that at $z/W = 0.5$ the $\delta_{99} = 0.01$, which is a similar value as the only fluid case. At $z/W = 0.4$ the values of Case A and C are extended again to the behind the edge of the first object at a value of 0.18, close to the edge of the object which end at 0.17. The flow is strong enough to create a very thin thermal layer at the edge of the flow. Case B and D have there δ_{99} inside the object at 0.078 and 0.61 respectively. These values are very close to their Ra = 10^6 counterparts.

6.3. Velocity contours

Figure 6.3 shows the velocity contours at Ra = $10^5, 10^6$ and 10^7. The velocity has the same normalization as in section 5.3. In the cases with the objects not attached to the walls all heat was transferred from the wall to the fluid and that is where the buoyancy force took place. Now much of that space is occupied by the objects that are attached to the walls. However, heat can flow through the object and be transferred to the fluid via the object and buoyancy can place at the sides of the object. This can have two consequences depending if the object is conducting or insulating.

- If the object at the wall is insulating it prevents heat from transferring through the object. Most heat is

still transferred through the wall to the fluid. But most space of the wall is occupied by the blocks and only 55 % of the wall is left to transfer heat to the fluid. The objects also block the flow and thus decrease circulation. This greatly diminishes heat transfer to the fluid and thus the buoyancy force. This can be seen best in the Case B cases who all have little flow.

- If the object is conducting heat is transferred from the wall into the object and to the fluid. This increases the surface area where heat can be transferred to by a factor of 2.8. This causes a huge increase of buoyancy force in between conducting objects. This is best noticed in Case A at Ra = 10^6 and 10^7 where a very large flow can be seen in plane $z/W = 0.5$ in between the objects at the edge.

Figure 6.4 shows the normalized Re as discussed in section 5.3 for all the cases. The Re is again normalized by Re_0, the Re of the only fluid case.

Velocity contours at Ra = 10^5

Figure 6.3a shows the velocity contours of the four cases with the objects attached to the walls at $z/L = 0.4$ and $z/L = 0.5$. When looking at the velocity contours of Case A it can be seen that the momentum boundary layer is moved from the wall to the edge of the first column of objects. This is because the conductive objects have the same temperature as the hot wall and heat up the fluid at their edge. There is also velocity created in between the objects just like in Case A where objects didn't touch the wall. Figure 6.4 also shows the highest increase in Re for this case because it has the most conductive objects at the wall of all cases. Case B almost show no velocity. When looking at plane $z/L = 0.5$ a small velocity can be seen at the walls. This is due to the buoyancy force created by the hot wall. But it is much smaller than the only fluid case. That is because the objects attached to the wall are insulating. Case C has a conducting object at the bottom. In plane $z/L = 0.5$ a buoyancy force between the objects at the bottom can be seen, similar to Case A but less in strength. However the second and third object from the bottom are insulating so unlike Case A the strength of the velocity doesn't increase but diffuses over space and decreases. Case D has an insulating object at the bottom and conductive objects at the middle. The contours show a momentum boundary layer at the edge of the objects but it only starts at the second object of the bottom where the objects become conductive. There is some velocity in between the objects, mostly the conductive ones.
6.4 shows the Re/Re_0 of the cavity which is calculated through the RMS velocity. It can be seen that the cases with the objects against the wall have higher Re for cases A, C and D than the for the same cases where objects don't touch the wall. Only Case B has a lower Re. This is because they have conductive objects at the wall which create more buoyancy force. Case B consist only of insulating materials at the wall that hinder heat transport from the wall to the fluid and thus has almost no buoyancy.

Velocity contours at Ra = 10^6

Figure 6.3b shows the velocity contours of the four cases with the objects attached to the walls at $z/L = 0.4$ and $z/L = 0.5$ with Ra = 10^6. In the cases A, C and D with Ra = 10^5 most velocity was created at the edge of the conductive objects attached to the walls. However, when looked at the temperature contours of Ra = 10^6 it can be seen that now the most velocity is created at the wall or in between conductive objects. This is because there is circulation in the cavity to drive cold water past the edge of heated conductive object.
This can be most prominently seen in Case A. Case A shows a very large velocity in between the walls when looking at the $z/L = 0.5$ plane, much larger in magnitude and along a larger region in the xy-plane than at Ra = 10^5. This increase is because the increased circulation forces fluid in between the conductive objects, where it is heated by the two surrounding objects and the wall. This creates a huge buoyancy force and flow. Which in turn increases the circulation. This can be seen back in Figure 6.4 which shows a Re/Re_0 of 1.29 for Case A. Indicating that there is more velocity than in the only fluid case.
Case B stills show a very low velocity. When comparing the velocity contours at Ra = 10^5 (figure 6.3a) and Ra = 10^6 almost no difference can be observed. However, when comparing the Re numbers, it shows there that at Ra = 10^6 the Re is less decreased compared to the only fluid case than at Ra = 10^5.
Case C has a conducting object at the bottom. In Case C with Ra = 10^5 there were no specific places with high velocity. However, when looking at plane $z/L = 0.5$ a high velocity between the objects at the bottom can be seen, similar to Case A but less in strength. The second and third object from the bottom are insulating so unlike Case A the strength of the velocity doesn't increase but diffuses over space and decreases. The velocity decreases a bit after the first object as it gets diffused before diminishing completely beyond the first object. Looking at the Re in figure 6.4 Case C has a similar average velocity as the only fluid case.

Case D has an insulating object at the bottom and when looking at the velocity contours in plane $z/L = 0.5$ only a small buoyancy force at the wall can be seen. The insulating object only reduces the flow by obstructing it. The flow at between the lowest objects look a bit similar to Case B only in Case D it is a bit stronger. This is because there is a larger flow overall in Case D, meaning that there is a stronger circulation and thus more fluid reaches the wall through the object. The second and third object from the bottom are conducting. When looking at plane $z/L = 0.5$ it can be seen that the velocity increases because heat is conducted through the objects heating up the fluid. This creates the overall larger flow and circulation in Case D compared to Case B. This is similar to the Ra = 10^5 Case D but with stronger circulation the flow now is able to penetrate between the objects. and be heated by the sides of the conductive objects and the wall.
Comparing the Re numbers at Ra = 10^5 and Ra = 10^6 in figure 6.4 two major differences can be seen. First, the values of the four cases at Ra = 10^5 are a lot closer to each other than at Ra = 10^6. Secondly, all cases at Ra = 10^5 are below the only fluid case while only two cases (B and D) at Ra = 10^6 are below the only fluid case, one is similar (Case C) and Case A shows a higher Re number than the only fluid case. This means that in Case A the flow is enhanced placing objects in the cavity.

Velocity contours at Ra = 10^7

Figure 6.3c shows the velocity contours of Ra = 10^7. There is an increase of velocity at the wall in all cases. This is because at Ra = 10^7 there is a lot circulation and the centrifugal force pushes the flow close to the walls. The same two aspect as in the Ra = 10^5 and 10^6 can be seen. Conductive objects create flow while insulating objects decrease flow. When looking at figure 6.4 it can be seen that Case A has now a Re almost twice as strong as the only fluid case. Case B has a very similar ratio to the empty Case as the Ra = 10^6 counterpart. Case C and D have Re in between. From this it can be concluded that Re/Re_0 increases long as there are conductive objects attached to the walls.

6.4. Heat transfer

Figure 6.5 shows the Nu number at the walls. In this figure the Nu is log scale plotted because the magnitudes of the Nu are vary very much depending on the place of the wall. The objects attached to the wall are included in the figure as some of the heat is transferred to the fluid through the objects. When the object is insulating it can be seen that there is almost no heat transferred to the fluid. This can be most clearly seen in Case B with only insulating objects attached to the wall. When the object is conducting heat is transferred to the fluid. At the bottom this is strongest and it decreases as y increases. At the corner and edges of the objects most heat is transferred as these places are surrounded by fluid from more sides. This is most clearly seen in Case A with only conducting objects at the wall.

Heat transfer at Ra = 10^5

The Nusselt contours of the hot wall at Ra = 10^5 can be observed in figure 6.5a. The first observation made is that the amount of heat extracted from the wall is a lot less than in the only fluid case. This can also be seen in Figure 6.6 which shows the average Nu at the wall.
When looking at Case A in figure 6.5a it can be seen that the Nu is the biggest at the objects. The conductive objects conduct heat through the object to the edge where it is transferred to the cold water. It can be seen that the objects closer to the bottom transfer more heat to the fluid because there is a higher temperature gradient there. At the walls however there is almost no Nu. This is because the cold water must pass high temperature objects attached to the wall and is heated up before reaching the wall. It can also be seen that the highest Nu values are seen at the corners of the objects. The corners of the objects are the places where the objects least obstruct the flow and thus increases natural convection taking place there. Also the corners of the objects are surrounded by the most amount of fluid and thus it loses more energy to the fluid. (The face of an object is surrounded at one side of the fluid, the edge of an object is surrounded at two sides by fluid and a corner is surrounded by three sides). When looking at figure 6.5a it can be seen that of all four cases Case A has the highest relative $\langle Nu \rangle / \langle Nu \rangle_0$ of 0.73, indicating that having conductive objects attached to the wall creates the most heat transfer.
Case B shows almost no Nu. This is because the insulating objects attached to the wall prevent the edge of the object from heating up. There is a little Nu at the wall but because the objects are blocking the flow they prevent the fluid from reaching the wall this is very small. This results in a very small total heat transfer which can be seen in figure 6.6a where Case 2 has a $\langle Nu \rangle / \langle Nu \rangle_0$ of 0.25. This indicates almost pure conduction and very low flow, which agrees with the velocity contours in figure 6.3a and low Re seen in figure 6.4.

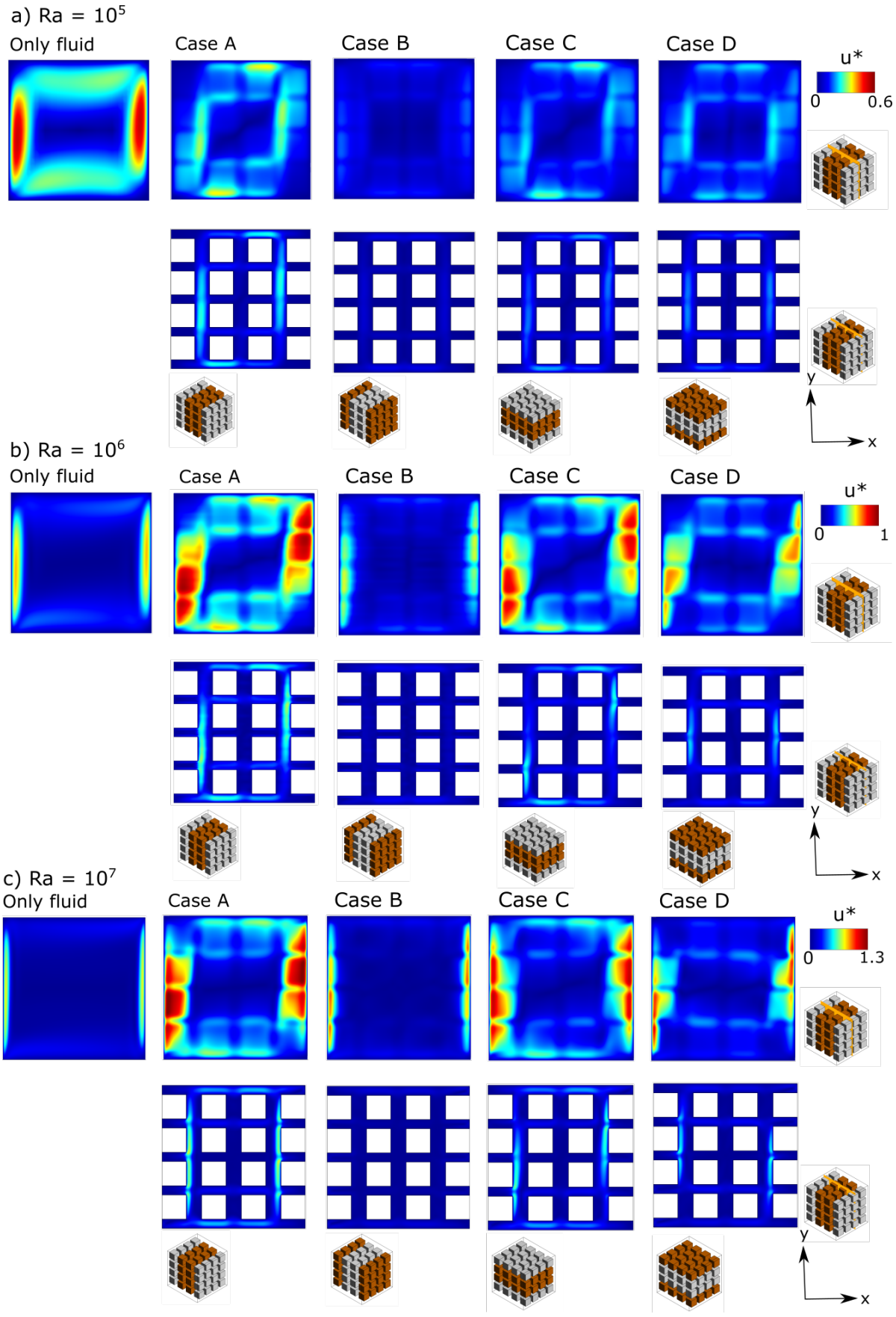

Figure 6.3: Velocity contours when objects are attached to the walls at a) Ra = 10^5, b) Ra = 10^6 and c) Ra = 10^7. The contours are taken at two planes, at $z/W = 0.5$ and $z/W = 0.4$.

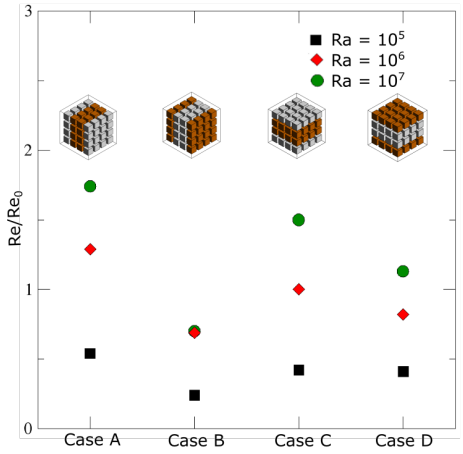

Figure 6.4: The Volume averaged RMS of Re when objects don't touch the walls. The Re is normalized by dividing to Re_0 of the only fluid case.

Case C and D have both have conductive and insulating objects. Just like in Case A the conductive objects show high Nu at the objects while the insulating objects show almost no Nu. Case D shows also Nu at the bottom of the wall while Case C doesn't. This is because Case C has conductive objects at the bottom so the fluid is already heated up before it reaches the wall. Case D has insulating objects at the wall so the fluid is not heated up. There is still flow in the cavity of Case D (unlike in Case B which also has insulating objects at the bottom) so the cold fluid reaches the wall at the bottom and is heated up. When looking at Figure 6.6 it is seen that they have both <Nu>/<Nu>$_0$ around 0.55

Heat transfer at Ra = 10^6

Figure 6.5b show the Nusselt contours at the hot wall at Ra = 10^6. Similar to the cases at Ra = 10^5 the conductive objects show high Nu, especially at the bottom and insulating show almost no Nu. However, the conductive objects show a considerable higher Nu. At Ra = 10^5 the conductive objects at the bottom showed a Nu between 10 at the faces and 60 at the corners and edges while at Ra = 10^6 the Nu is between the 25 and 75 is shown. Also at the bottom of all four cases a considerable increase in Nu can be seen. In the Nu contours of Ra = 10^5 only a small Nu could be seen at the wall of Case B and D and none at all in Case A and C. With Ra = 10^6 there is a Nu at the bottom of all the cases, a noticeably high one in Case D. This is because there is more circulation in the cavity with Ra = 10^6. This makes it possible for cold water to reach the hot wall which increases heat transfer between the wall and the fluid. The increased flow also increases heat transfer between conductive objects and the fluid.
When looking at the <Nu>/<Nu>$_0$ in figure 6.6. Case A shows the highest value in <Nu>/<Nu>$_0$ at 1.61. Most important thing about this <Nu> is that it has a higher value than 1. Meaning that adding objects in this case increases heat transfer through the cavity although the same temperature difference and length exist. Case B doesn't show an increase in <Nu>/<Nu>$_0$ while Case C and D show <Nu> around 1. Thus these cases have comparable heat transfer as the only fluid case.

Heat transfer at Ra = 10^7

In figure 6.5 the Nu contours at Ra = 10^7 can be seen. They look very similar to that of Ra = 10^6 but have a stronger magnitude. When looking at figure 6.6 it can be seen that Case A has twice the <Nu>/<Nu>$_0$ only fluid Case. Case B increases slightly to 0.5 and Case C and D increases to 1.4. This result is very similar as that of the Re numbers at Ra = 10^7. Thus it can be concluded that having conductive objects at the sides always increases the heat transfer at Ra = 10^7 and that a higher Rayleigh number increases this factor.

6.5. Thermal Disequilibrium

The thermal disequilibrium is calculated in the way described in section 5.5 and shown in figures 6.7, 6.8 and 6.9 for Ra = $10^5, 10^6$ and 10^7 respectively. Because the objects are attached to the wall one side is not

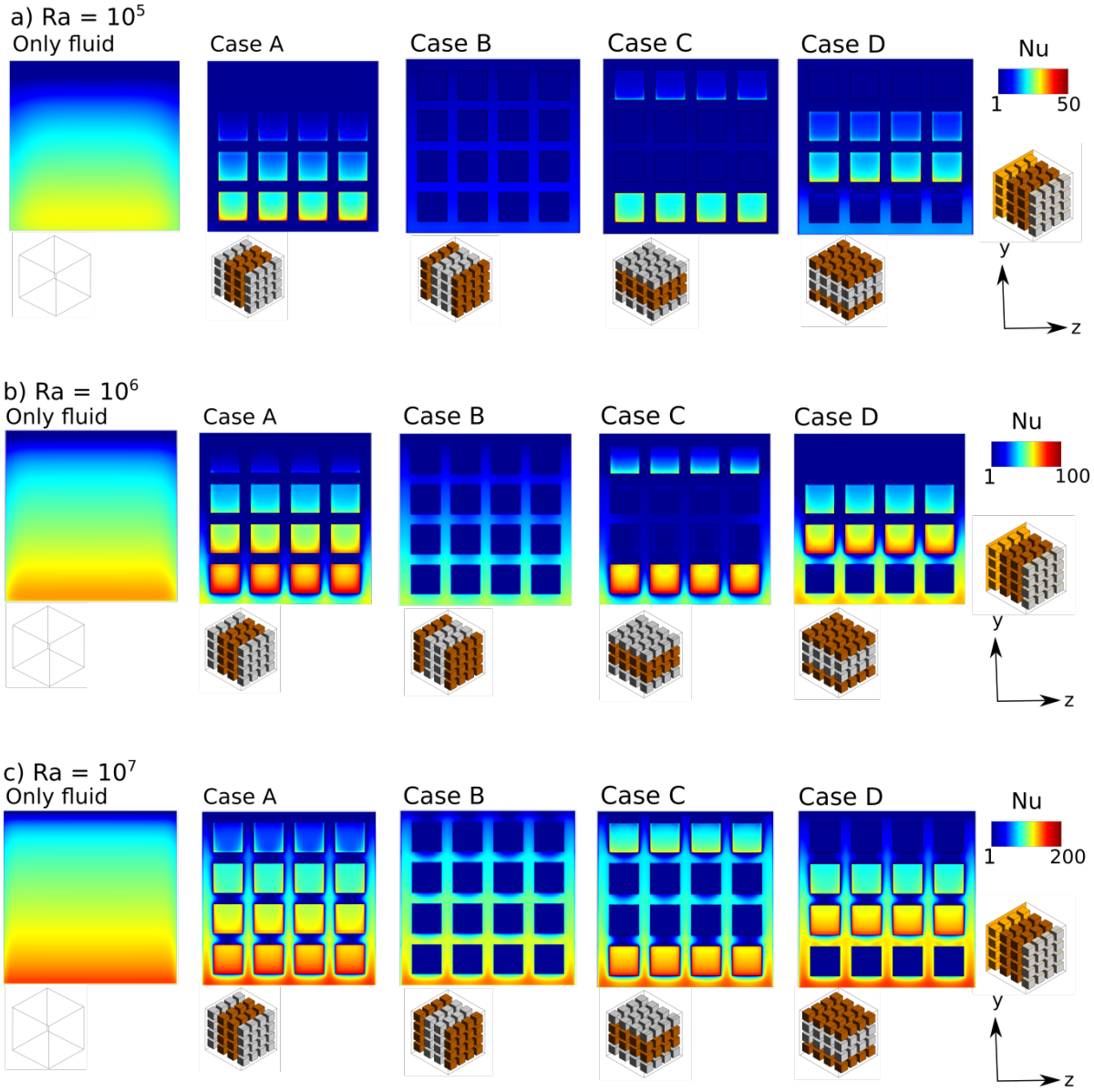

Figure 6.5: Nu contours at the hot wall and the objects attached them at a) Ra = 10^5, b) Ra = 10^6 and c) Ra = 10^7.

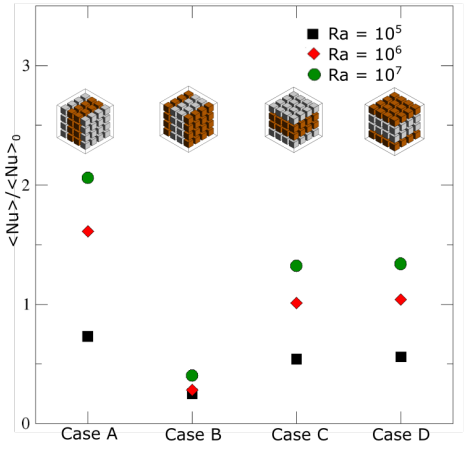

Figure 6.6: Average Nusselt number at the hot wall when objects are attached to the wall. The <Nu> is normalized by dividing over the <Nu> of the only fluid case.

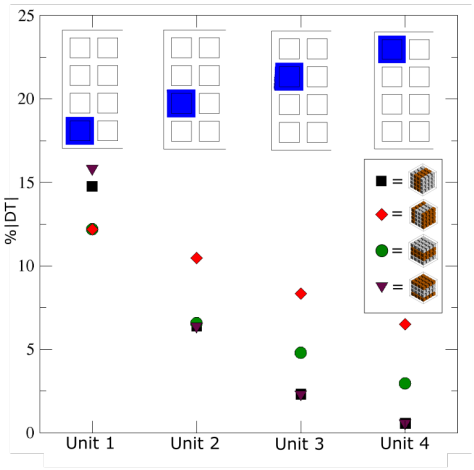

Figure 6.7: Thermal disequilibrium between objects and the fluid when the objects are attached the wall at Ra = 10^5.

surrounded by fluid anymore at the hot side of the object the $< T_f >$ is relative lower than the $< T_s >$. This results in overall higher DT values. Because the units are differently defined in the cases where the objects are not attached to the wall the DT values of this section and section 5.5 cannot be directly compared. However, the trends the DT follows can be compared.
There were two trends described in section 5.5.

1. Insulating objects show higher DT while conducting objects show low DT.

2. DT decreases as y increases.

When analyzing the DT for the cases with objects it will be seen that those trends are not all followed anymore.

Thermal Disequilibrium at Ra = 10^5

Figure 6.7 shows the DT at Ra = 10^5. When looking at Unit 1 it can be seen that all cases have high DT, even the conducting objects. This means that trend 1 is not anymore followed. This is because in the case of the objects not attached to the walls the objects assumed the average temperature of its surrounding fluid creating very low DT. In the case of objects touching the wall the conductive objects assume the temperature of the wall which creates high DT while the surrounding fluid can still contains cold fluid, especially the bottom units.
The DT at Unit 1 is the highest and decreases as the Unit is at a higher y. Thus trend 2 is still followed. This makes sense as the temperature varies less at the top of the cavity as the fluid is heated at that stage. It can be seen that Case B this decrease is much slower than the other cases. This is because there is almost no flow in Case B so much less heat is convected upwards, thus still maintaining a temperature difference across the upper units.

Thermal Disequilibrium at Ra = 10^6

Figure 6.8 shows the DT at Ra = 10^6. The DT in all cases has increased, especially in the lower Units. This is because higher Ra means more circulation. With the objects attached to the wall the units are also close to the wall and thus there is more moving fluid in the Units. For the lower Units this means that there is more cold fluid and thus higher DT. When looking at Unit 1 Case B shows much less DT than the other cases. This is Case B has dampened circulation due to the insulating objects at its walls. In Unit 2 Case D shows higher DT because in Case D the buoyancy force starts at Unit 2 and thus higher velocity.

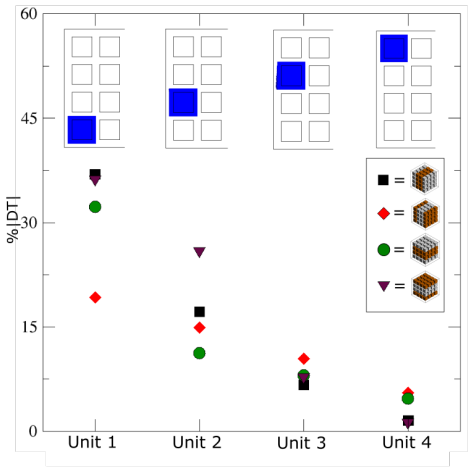

Figure 6.8: Thermal disequilibrium between objects and the fluid when the objects are attached the wall at Ra = 10^6.

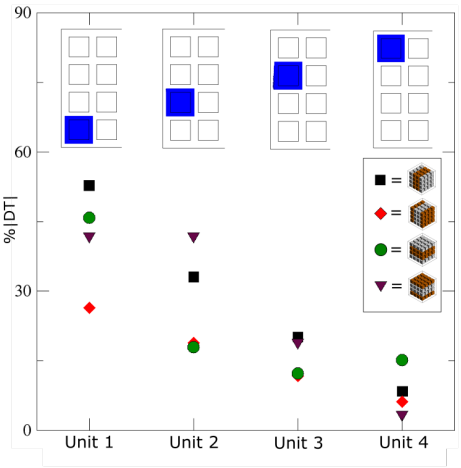

Figure 6.9: Thermal disequilibrium between objects and the fluid when the objects are attached the wall at Ra = 10^7.

Thermal disequilibrium at Ra = 10^7

Figure 6.9 shows the DT at Ra = 10^7. The DT is very high, up to 53% in Unit 1. When considering the temperature contours in figure 6.1c and comparing the $z/L = 0.4$ and the $z/L = 0.5$ plane at the regions where the Units are defined it can be seen that the temperature difference is very high at these regions. The circulation is so strong that the hot object in Unit 1 is almost completely surrounded by cold fluid, creating these high DT's.
It can be concluded that trend 2 still holds. There is also a new trend: the DT increases as Ra increases.

6.6. Summary and conclusion

Numerical simulations have been done at Ra = $10^5, 10^6$ and 10^7 for Case A to D with objects attached to the hot and cold wall. The objects at the wall block the flow considerably and prevent the cold water from reaching the hot wall in Ra = 10^5. In Ra = 10^6 and 10^7 the flow is strong enough to reach the wall. Conductive objects strongly increase the buoyancy force as they increase the area they can transfer heat to the fluid. At Ra = 10^6 and 10^7 Case A, who only has conductive objects at the wall has a Re and <Nu> higher then the only fluid case. Insulating objects reduce the buoyancy force as they reduce the area at the wall heat can be transferred to the fluid and also obstruct the flow ot the wall.

7

Conclusion

The research has been done on four different configurations of insulating and conducting objects in a side heated cavity at Ra $10^5, 10^6$ and 10^7. The four cases were studied when the objects were not attached to the wall and when they were attached to the wall. First the conclusions are discussed when the objects are unattached from the wall and then the results are discussed when they are attached to the wall.

7.1. Objects not attached to the wall

Objects are at a small distance from the wall. It depends if on the Ra if the objects are within the thermal boundary layer if they influence the flow. Ra = 10^5 is within this region and different behaviour can be seen between the four configurations. Conductive objects show a higher Nu at the wall indicating they stimulate heat transfer while insulating objects decrease the Nu at the wall. Case A, who only has conductive objects at the wall shows more flow in between the objects as the objects extract more heat from the walls and increase the buoyancy force around them. Case B, who only has insulating objects at the wall shows more flow at the wall because the objects create a strong temperature gradient there. Case B has a smaller <Nu> at the wall than the rest of the cases. Thus having only insulating objects at the wall decreases heat transfer. Case A, C and D have a similar <Nu> which is higher than B. These cases have conductive objects at the wall which increases heat transfer. Case C and D also have insulating objects at the wall thus the increase of heat transfer due to conducting objects is stronger than the decrease due to insulating objects. Also that the increase of heat transfer due to conductivity due to conducting blocks stops at a certain number of blocks.
At Ra = 10^6 the objects are not anymore within the thermal boundary layer and no difference can be seen between the four cases when looked at the velocity field and <Nu> values but the objects still slow down the flow thus the cases have lower <Nu> and Re values. At Ra = 10^7 all the objects are almost entirely in the stagnant center of the cavity and the velocity field, temperature profile and <Nu> are very similar to the only fluid case.

7.2. Objects attached to the walls

When the objects are attached to the wall the influence is very different. The objects are always situated in the thermal boundary layer. Heat can also directly flow into the objects from the wall. In case of conductive objects heat is transferred via the object to its surrounding fluid creating a strong buoyancy force in between the objects. Conductive objects thus vastly increase the heat transfer. Insulating objects however don't transfer a lot of heat from the wall to the objects and block the flow, preventing it from reaching the wall. Insulating objects thus decrease heat transfer. Case A shows the most increase in heat transfer as it has only conductive objects. At a Ra of 10^5 the heat transfer is still lower as the only fluid case as the objects also block the flow. However, at Ra of 10^6 and 10^7 Case A show <Nu> higher than that of the only fluid case, showing that the heat transfer from the left to the right of the cavity is effectively increased by adding conductive objects. Case B, which has only insulating objects at the wall results in reduced heat transfer. Case C and D, which has 50% conductive and 50% insulating objects at the walls show heat transfer comparable to the only fluid case at Ra = 10^6. At Ra = 10^7 the heat transfer is higher than the only fluid case, showing that the increasing effect of the conductive objects have more influence than the decreasing effect of the insulating objects.

At a Ra 10^6 and 10^7 the circulation becomes so strong that the conductive objects cannot heat the surrounding fluid in time to make it the same temperature, creating large thermal disequilibriums at these places.

8

Recommendation

- Only two distances between the wall and the objects have been researched. Chapter 5 the objects are at a distance $x/L = 0.03$ and in chapter 6 the objects are touching the wall. In chapter 5 the cases at a Ra of 10^6 and 10^7 show little influence of the objects because the thermal boundary layer of does not reach the objects. Thus the distance between the wall and the object is of big influence. A more quantitative study between distances of conductive objects can be done. Hypothetically, the effect of conductive objects should get stronger the closer the objects are to the wall because the thermal resistance of the fluid between the wall and the object decreases.
- When there are conductive objects attached to the wall they increase the heat transfer compared to only fluid case. This could be very useful in enhancing heat transport in porous medium. Merrikh and Lage[15] and Raji [16] concluded that the natural convection decreases as the number of objects N increases. It could be useful to do an investigation at what number of objects N the enhancement of natural convection is not anymore stronger than the blocking effect of the objects. This can be done by doing a numerical simulation with conducting objects at the wall, but varying the number of objects.
- Conductive objects at an Ra of 10^5 when the objects are at a close distance to the wall and at all Ra researched when the objects are attached to the wall all show an increase in Nu at the wall. However, this effect is stronger when the object is placed at the bottom of the wall and its effect decreases as y increases. Case C and D have both insulating and conducting objects but have similar <Nu>. This is because the conducting objects are placed at the top and bottom in Case C, thus one object shows a lot of influence and one very little. While in Case C the conducting objects are placed in the middle positions and thus have both average influence. It would be interesting to study the exact influence of the position of the conducting block. A suggested method is to have only 1 conducting object at the wall and vary this object with y.

A

Governing equations

A.1. Differential conservation law

Every fluid flow can be described by the conservation of mass, momentum and internal energy. Suppose we have control volume X, then the change of extensive property Φ can be described by:

$$\text{Change of } \Phi_X = \text{influx of } \Phi_{in} - \text{outflux of } \Phi_{out} + \text{production} \tag{A.1}$$

It is however more useful to work with intensive property ϕ as it doesn't change with volume. Φ is the volume integral of ϕ while the in- and out-flux of Φ is the surface integral of ϕ times the velocity in the normal direction of the surface. Putting that in mathematical terms results in the integral form of the general conservation law.

$$\int_X \frac{\partial \phi}{\partial t} dV = -\int_{A_X} \phi u_j dA_j + \int_X \dot{\gamma}_P dV \tag{A.2}$$

Property ϕ can be substituted for ρ in the conservation of mass balance, ρv_j for the conservation of momentum balance and ρe for the conservation of energy balance. To get to a differential form of the conservation law Green-Gauss theorem can be used to describe the in- and out-flux as a volume integral instead of a surface integral:

$$\int_{A_X} \phi v_j dA_j = \int_X \frac{\partial}{\partial x_j}(\phi u_j) dV \tag{A.3}$$

Substituting that in A.2 gives us:

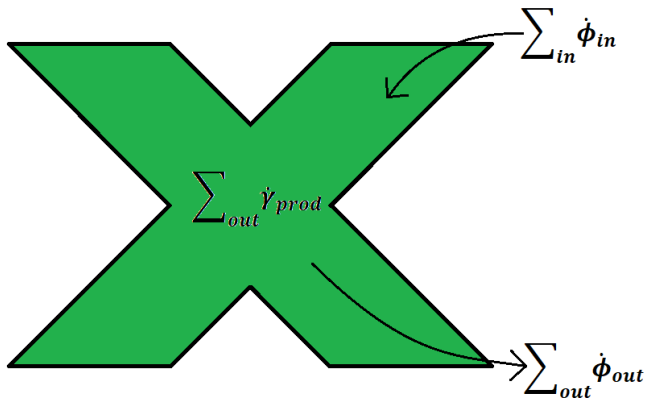

Figure A.1: Control Volume X

$$\int_X \frac{\partial \phi}{\partial t} dV = -\int_X \frac{\partial}{\partial x_j}(\phi u_j) dV + \int_X \dot{\gamma_P} dV$$

Now everything is in the same volume integral the integral signs can be omitted.

$$\frac{\partial \phi}{\partial t} = -\frac{\partial}{\partial x_j}(\phi u_j) + \dot{\gamma_P} = -u_j \frac{\partial \phi}{\partial x_j} - \phi \frac{\partial u_j}{\partial x_j} + \dot{\gamma_P} \tag{A.4}$$

From here on it is useful to follow the property from a langrangian perspective, but translated to an euleuran coordintate perspective. This allows for making force or energy balances on the control volume while the control volume moves with along the fluid that moves with velocity u_j. An easy way to do this is to use the material derivative which is defined as:

$$\frac{D}{Dt} = \frac{\partial}{\partial t} + u_j \frac{\partial}{\partial x_j} \tag{A.5}$$

By shuffling equation A.4 it is possible to form a balance equation of property ϕ in langrangian perpective.

$$\frac{D\phi}{Dt} = \frac{\partial \phi}{\partial t} + u_j \frac{\partial \phi}{\partial x_j} = -\phi \frac{\partial u_j}{\partial x_j} + \dot{\gamma_P} \tag{A.6}$$

A.2. Continuity equation

From equation A.4 the continuity equation can be derived by substituting ϕ with ρ. Because there is no production of mass in a control volume unless there is a nuclear reaction or God performs a miracle, $\dot{\gamma_P}$ is 0. This results in the continuity equation.

$$\frac{D\rho}{Dt} = \frac{\partial \rho}{\partial t} + u_j \frac{\partial \rho}{\partial x_j} = -\rho \frac{\partial u_j}{\partial x_j} \tag{A.7}$$

If the fluid density is constant or incompressible the material derivative will not change with time so $\frac{D\rho}{Dt} = 0$. This reduces the equation to.

$$\frac{\partial u_j}{\partial x_j} = \frac{\partial u}{\partial x} + \frac{\partial v}{\partial y} + \frac{\partial w}{\partial z} = 0 \tag{A.8}$$

A.3. Navier-Stokes equation

A momentum balance can be derived by substituting ϕ by ρv_i in the general conservation law.

$$\frac{D\rho u_i}{Dt} = \rho \frac{Du_i}{Dt} + u_i \frac{D\rho}{Dt} = -\rho u_i \frac{\partial u_j}{\partial x_j} + \dot{\gamma_P}$$

The continuity equation A.7 can be used to substitute $\frac{D\rho}{Dt}$ with $-\rho \frac{\partial u_j}{\partial x_j}$. The exact same term is present at the right hand side of the equation and they thus cancel and from its ashes the Cauchy momentum equation emerges.

$$\frac{D\rho u_i}{Dt} = \rho \frac{Du_i}{Dt} - u_i \rho \frac{\partial u_j}{\partial x_j} = -\rho u_i \frac{\partial u_j}{\partial x_j} + \dot{\gamma_P}$$

$$\rho \frac{Du_i}{Dt} = \rho \frac{\partial u_i}{\partial t} + \rho u_j \frac{\partial u_i}{\partial x_j} = \dot{\gamma_P} \tag{A.9}$$

The production $\dot{\gamma_P}$ of the momentum is caused by the gravity ρg_i and the Cauchy stress tensor σ_{ij}.

$$\dot{\gamma_P} = \rho g_i + \frac{\partial \sigma_{ij}}{\partial x_j}$$

The Cauchy stress tensor is a sum of viscous stress, pressure and elastic stress. In fluids the elastic stress can be neglected and the pressure is only present in the normal direction of the tensor.

$$\sigma_{ij} = -P * \delta_{ij} + \epsilon_{ij}$$

The viscous stress is really hard to exactly describe, luckily most fluids used for practical purposes are Newtonian fluids where the stress is linearly dependent on the local strain rate. Or in math terms $\epsilon = \mu\frac{\partial u}{\partial y}$. Newtonian fluids have two important assumptions. 1. The viscosity constant is isotropic. 2. The viscous stress is symmetric. Applying these two assumptions the resulting viscous stress will look like this:

$$\epsilon_{ij} = \mu(\frac{\partial u_i}{\partial x_j} + \frac{\partial u_j}{\partial u_i} - \frac{2}{3}\frac{\partial u_k}{\partial x_k}\delta_{ij}) \tag{A.10}$$

Filling everything in in equation A.9 we get the Naviern Stokes equation:

$$\rho\frac{Du_i}{Dt} = \rho g_i + \frac{\partial}{\partial x_j}(\mu(\frac{\partial u_i}{\partial x_j} + \frac{\partial u_j}{\partial u_i} - (\frac{P}{\mu} + \frac{2}{3}\frac{\partial u_k}{\partial x_k})\delta_{ij})) \tag{A.11}$$

If the fluid is assumed to have constant density $\frac{\partial u_k}{\partial x_k} = 0$ and the viscous stress tensor reduces to:

$$\epsilon_{ij} = \mu(\frac{\partial u_i}{\partial x_j} + \frac{\partial u_j}{\partial u_i})$$

When put into the Navier Stokes equation A.11 you get:

$$\rho\frac{Du_i}{Dt} = \rho g_i + \frac{\partial}{\partial x_j}(\mu(\frac{\partial u_i}{\partial x_j} + \frac{\partial u_j}{\partial x_i} - \frac{P}{\mu}\delta_{ij}))$$

$\frac{\partial}{\partial x_j}P\delta_{ij}$ is equal to the gradiant of P and can be shortend to $-\frac{\partial P}{\partial x_i}$ and $\frac{\partial}{\partial x_j}(\frac{\partial u_j}{\partial x_i}) = \frac{\partial}{\partial x_i}(\frac{\partial u_j}{\partial x_j}) = 0$ in case of an incompressible fluid. It is also assumed that the viscousity is constant so that it can be put for the divergence term. This gives us finally the incompressible newtonian fluid version of the N.S.

$$\rho\frac{Du_i}{Dt} = \rho g_i - \frac{\partial P}{\partial x_i} + \mu\frac{\partial^2 u_i}{\partial x_j^2} \tag{A.12}$$

It is useful to use the dynamic pressure[38]:

$$\frac{\partial P_{dynamic}}{\partial x_i} = \frac{\partial P}{\partial x_i} - \rho_0 g$$

The Boussinesq approximation is used to make the expansion of the fluid linear to the temperature difference.

$$\rho - \rho_\infty = \beta(T_\infty - T) \tag{A.13}$$

Filing the Boussinesq in A.12 gives the Navier Stokes used in this report.

$$\rho\frac{Du_i}{Dt} = \beta(T_\infty - T)g_i - \frac{\partial P}{\partial x_i} + \mu\frac{\partial^2 u_i}{\partial x_j^2} \tag{A.14}$$

A.4. Energy equation

By substituting ϕ in the general conservation law A.4 with ρe the energy equation can be derived.

$$\frac{D\rho e}{Dt} = \rho\frac{De}{Dt} + e\frac{D\rho}{Dt} = -\rho e\frac{\partial u_j}{\partial x_j} + \dot{\gamma_P}$$

Using the same trick that is used with the Navier-Stokes equation. $\frac{D\rho}{Dt}$ is substituted with $-\rho\frac{\partial u_j}{\partial x_j}$ and both terms on left and right side are cancelled.

$$\frac{D\rho e}{Dt} = \rho\frac{De}{Dt} - \rho e\frac{\partial u_j}{\partial x_j} = -\rho e\frac{\partial u_j}{\partial x_j} + \dot{\gamma_P}$$

$$\rho\frac{De}{Dt} = \rho\frac{\partial e}{\partial t} + \rho u_j\frac{\partial e}{\partial x_j} = \dot{\gamma_P} \tag{A.15}$$

The energy production term $\dot{\gamma_P}$ is made up out of thermal conduction, internal heat generation and net work from the environment to the control volume.[25]

$$\dot{\gamma_P} = -\frac{\partial q_i''}{\partial x_i} + q''' + \sigma_{ij}\frac{\partial u_i}{\partial x_j}$$

Conduction q_i'' is defined as $-k\frac{\partial T}{\partial x_i}$. Energy production from the net work depends on the stress tensor and can be divided in two parts. The normal volume change expressed by $-P\frac{\partial u_i}{x_i}$ and the viscous dissipation $\mu\Psi$. Putting everything in gives equation A.15.

$$\rho\frac{De}{Dt} = \frac{\partial}{\partial x_i}k\frac{\partial T}{\partial x_i} + q''' + P\frac{\partial u_i}{x_i} + \mu\Phi \tag{A.16}$$

Phi is the viscous dissipation function and can be expressed as:

$$\Phi = \frac{\partial u_i}{\partial x_j}\frac{\partial u_j}{\partial x_j} - \frac{2}{3}\frac{\partial u_i}{\partial x_i}\frac{\partial x_i}{\partial x_j}\text{[39]}$$

It is more useful to express the energy equation in terms of Temperature. To do that we first express the energy equation in enthalpy: $h = e + \frac{P}{\rho}$. Taking the material derivative of h we get

$$\frac{Dh}{Dt} = \frac{De}{Dt} + \frac{D}{Dt}\frac{P}{\rho} = \frac{De}{Dt} + \frac{1}{\rho}\frac{DP}{Dt} - \frac{P}{\rho^2}\frac{D\rho}{Dt}$$

replacing e with h and $\frac{D\rho}{Dt}$ with $\rho\frac{\partial u_i}{\partial x_i}$ in equation A.16 gives:

$$\rho\frac{Dh}{Dt} = \frac{\partial}{\partial x_i}\left(k\frac{\partial T}{\partial x_i}\right) + q''' + P\frac{\partial u_i}{x_i} + \mu\Phi + \frac{DP}{Dt} - P\frac{\partial u_i}{x_i}$$

$$\rho\frac{Dh}{Dt} = \frac{\partial}{\partial x_i}k\frac{\partial T}{\partial x_i} + q''' + \mu\Phi + \frac{1}{\rho}\frac{DP}{Dt} \tag{A.17}$$

The change of enthalpy ds can be expressed in:

$$dh = Tds + \frac{1}{\rho}dP \tag{A.18}$$

Where ds is the change of entropy. The change of entropy is:

$$ds = \left(\frac{ds}{dT}\right)_P + \left(\frac{\partial s}{\partial P}\right)_T dP$$

Maxwell's relationships gives us:

$$\left(\frac{\partial s}{\partial P}\right)_T = -\left(\frac{\partial}{\partial T}\frac{1}{\rho}\right]_P = -\frac{\beta}{\rho}$$

$$-\frac{1}{\rho}\left(\frac{\partial \rho}{\partial T}\right)_P$$

$$\left(\frac{\partial s}{\partial T}\right)_P = \frac{c_P}{T}$$

With β being the thermal expansion coefficient. When filling all terms in eq A.18 it gives us.

$$dh = c_P dT + \frac{1}{\rho}(1-\beta T)dP \tag{A.19}$$

When taking the material derivative of H and putting it in the energy equation eq A.17 it gives us the temperature formulation of the energy equation.

$$\rho c_P\frac{DT}{Dt} + (1-\beta T)\frac{DP}{Dt} = \frac{\partial}{\partial x_i}k\frac{\partial T}{\partial x_i} + q''' + \mu\Phi + \frac{DP}{Dt}$$

$$\rho c_P\frac{DT}{Dt} = \frac{\partial}{\partial x_i}k\frac{\partial T}{\partial x_i} + q''' + \mu\Phi + \beta T\frac{DP}{Dt} \tag{A.20}$$

In the cases that are investigated in this report there is no energy production. The heat generated through viscosity is neglected. The fluid is assumed to be incompressible ($\beta = 0$) except for the buoyancy term. ρ, k and c_P are assumed to be constant. This simplifies the energy equation to.

$$\rho c_P \frac{DT}{Dt} = k \frac{\partial^2 T}{\partial x_i^2} \tag{A.21}$$

B

Non-dimensional numbers

In heat transfer it is very useful to define the problem in non-dimensional numbers. So to clearly see what physical parameters dominate over each other. The following non-dimensional numbers are used in this report:

Reynolds number

The Reynolds number is defined as:

$$Re = \frac{UL}{\nu} = \frac{inertial\ force}{viscous\ force} \tag{B.1}$$

The Reynolds number is the ratio of the inertial force over the viscous force. A higher Reynolds number means a bigger momentum and a stronger flow. At low Re the flow is laminar while at high Re the flow is turbulent. The Re the flow becomes turbulent is called Re_{cr} and is fixed for each geometry. It is thus a very useful non-dimensionless number to predict if you are going to have laminar or turbulent flow.

Prandtl number

$$Pr = \frac{\nu}{\alpha} = \frac{viscous\ diffusion}{thermal\ diffusion} \tag{B.2}$$

The Prandtl number is the ratio of viscous diffusion over thermal diffusion. A high Pr means a faster diffusion of motion while a low Pr means a faster diffusion of heat. This is very useful while analyzing the boundary layer. A high Pr means high thermal diffusion and thus a small thermal boundary layer compared to the viscous boundary layer while a low Pr gives a small viscous boundary layer due to fast diffusion of movement.

Rayleigh number

$$Ra = \frac{\beta \Delta T g L^3}{\alpha \nu} = \frac{buoyancy\ force}{diffusive\ force} \tag{B.3}$$

The buoyancy force is the driving force of natural convection The Rayleigh numbers is thus an excellent way to quantify the strength of natural convection in a system. A higher Rayleigh number means stronger natural convection. At very strong natural convection the flow will turn turbulent and just like the Reynolds number, the Rayleigh number is a good way to estimate this transition.

Nusselt number

$$Nu = \frac{hL}{\lambda} = \frac{convective\ heat\ transfer}{conductive\ heat\ transfer} \tag{B.4}$$

The Nusselt number shows if the heat transfer within a fluid is convection dominated or conduction dominated. Because λ stays most of the cases constant it is a good measurement of the strength of the convection. Nu = 1 means pure conduction and the higher the Nusselt number the more convection there is.

C

Nusselt numbers

Here is an overview of all the Nusselt numbers from all the cases when the objects are not attached to the wall:

Table C.1: The Nu numbers when the objects are not attached to the wall.

Raileigh number	Fluid-only case	Case A	Case B	Case C	Case D
Ra = 1.5×10^5	5.1	2.41	1.60	2.27	2.34
Ra = 1.5×10^6	10.2	7.89	7.62	7.98	7.88
Ra = 1.5×10^7	19.48	18.25	18.22	18.45	18.77

Here is an overview of all the Nusselt numbers when the objects are attached to the wall:

Table C.2: The Nu numbers when the objects are attached to the wall.

Raileigh number	Fluid-only case	Case A	Case B	Case C	Case D
Ra = 1.5×10^5	5.1	3.74	1.29	2.74	2.86
Ra = 1.5×10^6	10.2	16.43	3.04	10.33	10.61
Ra = 1.5×10^7	19.48	40.20	7.86	25.88	26.21

Bibliography

[1] Y. Tian and C. Y. Zhao. A review of solar collectors and thermal energy storage in solar thermal applications. *Applied Energy*, 2013. ISSN 03062619. doi: 10.1016/j.apenergy.2012.11.051.

[2] Huili Zhang, Jan Baeyens, Gustavo Cáceres, Jan Degrève, and Yongqin Lv. Thermal energy storage: Recent developments and practical aspects, 2016. ISSN 03601285.

[3] Salmaan Craig and Jonathan Grinham. Breathing walls: The design of porous materials for heat exchange and decentralized ventilation. *Energy and Buildings*, 2017. ISSN 03787788. doi: 10.1016/j.enbuild.2017.05.036.

[4] Abdul Ravoof Shaik, Sheik S. Rahman, Nam H. Tran, and Thanh Tran. Numerical simulation of Fluid-Rock coupling heat transfer in naturally fractured geothermal system. *Applied Thermal Engineering*, 2011. ISSN 13594311. doi: 10.1016/j.applthermaleng.2011.01.038.

[5] K. A.R. Ismail and R. Stuginsky. Parametric study on possible fixed bed models for pcm and sensible heat storage. *Applied Thermal Engineering*, 1999. ISSN 13594311. doi: 10.1016/S1359-4311(98)00081-7.

[6] A. F. Mills. *Basic Heat and Mass Transfer*. Prentice Hall Inc, Los Angeles, 2 edition, 1999. ISBN 0-13-096247-3.

[7] Iman Ataei-Dadavi, Nima Rounaghi, Manu Chakkingal, Sasa Kenjeres, Chris R. Kleijn, and Mark J. Tummers. An experimental study of flow and heat transfer in a differentially side heated cavity filled with coarse porous media. *International Journal of Heat and Mass Transfer*, 143:118591, 11 2019. ISSN 00179310. doi: 10.1016/j.ijheatmasstransfer.2019.118591. URL `https://linkinghub.elsevier.com/retrieve/pii/S0017931019312955`.

[8] Jan Erik Weber. The boundary-layer regime for convection in a vertical porous layer. *International Journal of Heat and Mass Transfer*, 18(4):569–573, 1975. ISSN 00179310. doi: 10.1016/0017-9310(75)90298-7.

[9] G. Lauriat and V. Prasad. Non-Darcian effects on natural convection in a vertical porous enclosure. *International Journal of Heat and Mass Transfer*, 32(11):2135–2148, 1989. ISSN 00179310. doi: 10.1016/0017-9310(89)90120-8.

[10] N. Seki, S. Fukusako, and H. Inaba. Heat transfer in a cavity packed with fibrous glass. *Journal of Heat Transfer*, 100(4):748–750, 1978. ISSN 15288943. doi: 10.1115/1.3450896.

[11] John M. House, Christoph Beckermann, and Theodore E. Smith. Effect of a centered conducting body on natural convection heat transfer in an enclosure. *Numerical Heat Transfer; Part A: Applications*, 18(2):213–225, 1990. ISSN 15210634. doi: 10.1080/10407789008944791.

[12] M. M. Mousa. Modeling of Laminar Buoyancy Convection in a Square Cavity Containing an Obstacle. *Bulletin of the Malaysian Mathematical Sciences Society*, 39(2):483–498, 4 2016. ISSN 21804206. doi: 10.1007/s40840-015-0188-z.

[13] Prasad Bhave, Arunn Narasimhan, and D.A.S. Rees. natural convection heat transfer enhancement using adiabatic block. *International Journal of Heat and Mass Transfer*, 49:3807–3818, 2006.

[14] R. Roslan, H. Saleh, and I. Hashim. Natural convection in a differentially heated square enclosure with a solid polygon. *Scientific World Journal*, 2014. ISSN 1537744X. doi: 10.1155/2014/617492.

[15] Ali A. Merrikh and José L. Lage. Natural convection in an enclosure with disconnected and conducting solid blocks. *International Journal of Heat and Mass Transfer*, 48(7):1361–1372, 3 2005. ISSN 00179310. doi: 10.1016/j.ijheatmasstransfer.2004.09.043.

[16] A. Raji, M. Hasnaoui, M. Naïmi, K. Slimani, and M. T. Ouazzani. Effect of the subdivision of an obstacle on the natural convection heat transfer in a square cavity. *Computers and Fluids*, 68:1–15, 9 2012. ISSN 00457930. doi: 10.1016/j.compfluid.2012.07.014.

[17] K. Hooman and A. A. Merrikh. Theoretical Analysis of Natural Convection in an Enclosure Filled with Disconnected Conducting Square Solid Blocks. *Transport in Porous Media*, 85(2):641–651, 11 2010. ISSN 01693913. doi: 10.1007/s11242-010-9583-y.

[18] G. De Vahl Davis. Natural convection of air in a square cavity: A bench mark numerical solution. *International Journal for Numerical Methods in Fluids*, 3(3):249–264, 1983. ISSN 10970363. doi: 10.1002/fld.1650030305.

[19] N. Ramesh and S. P. Venkateshan. Effect of surface radiation on natural convection in a square enclosure. *Journal of thermophysics and heat transfer*, 13(3):299–301, 1999. ISSN 08878722. doi: 10.2514/2.6458.

[20] F. Ampofo and T. G. Karayiannis. Experimental benchmark data for turbulent natural convection in an air filled square cavity. *International Journal of Heat and Mass Transfer*, 46(19):3551–3572, 2003. ISSN 00179310. doi: 10.1016/S0017-9310(03)00147-9.

[21] M. Hortmann, M. Peric, and G. Scheuerer. Finite volume multigrid prediction of laminar natural convection: Bench???mark solutions. *International Journal for Numerical Methods in Fluids*, 1990. doi: 10.1002/fld.1650110206.

[22] Osman Turan, Nilanjan Chakraborty, and Robert J. Poole. Laminar natural convection of Bingham fluids in a square enclosure with differentially heated side walls. *Journal of Non-Newtonian Fluid Mechanics*, 165(15-16):901–913, 8 2010. ISSN 03770257. doi: 10.1016/j.jnnfm.2010.04.013.

[23] R. A.W.M. Henkes and P. Le Quéré. Three-dimensional transition of natural-convection flows. *Journal of Fluid Mechanics*, 319:281–303, 7 1996. ISSN 00221120. doi: 10.1017/S0022112096007343.

[24] Fusegi T, Hyun J.M, Kuwahara K, and Farouk B. a numerical study of three-dimensional natural convection in a differentially heated cubical enclosure. *Heat Mass Transfer*, 34, 1991.

[25] Adrian Bejan. *Converction heat transfer*. John Wiley & Sons, 3rd edition, 2004.

[26] Nima Rounaghi. Side Heated Natural convection in coarse-grained porous media. Technical report, TU-Delft, 2018.

[27] Donald A Nield and Adrian Bejan. *Convection in Porous Media*. Springer, 5 edition, 2006.

[28] Fluent 6.3 User's Guide: General Scalar Transport Equation, 2006. URL `https://www.sharcnet.ca/Software/Fluent6/html/ug/node989.htm`.

[29] Praveen. C. Finite volume method on unstructured grids-lecture, 2013.

[30] Fluent 6.3 User's Guide: Evaluation of Gradients and Derivatives, 2006. URL `https://www.sharcnet.ca/Software/Fluent6/html/ug/node994.htm`.

[31] Hanjalic K., Kenjeres S., Tummers M.J., and Jonker H.J.J. *Analysis and Modelling of Physical Transport Phenomena*. VSSD, 2006.

[32] Fluent 6.3 User's Guide: Spatial Discretization. 2006. URL `https://www.sharcnet.ca/Software/Fluent6/html/ug/node992.htm`.

[33] Ansys Fluent 12.0 Theory Guide: Discretization of the Momentum Equation, 2006. URL `http://www.afs.enea.it/project/neptunius/docs/fluent/html/th/node371.htm`.

[34] ANSYS. Choosing the Pressure-Velocity Coupling Method, 2009. URL `http://www.afs.enea.it/project/neptunius/docs/fluent/html/ug/node785.htm`.

[35] Olga Shishkina, Richard Jam Stevens, Siegfried Grossmann, and Detlef Lohse. Boundary layer structure in turbulent thermal convection and its consequences for the required numerical resolution. *New Journal of Physics*, 12, 7 2010. ISSN 13672630. doi: 10.1088/1367-2630/12/7/075022.

[36] Bernard Castaing, Stephane Zaleski, Gemunu Gunaratne, Leo Kadanoff, Albert Libchaber, Xiao Zhong Wu, Gianluigi Zanetti, François Heslot, and Stefan Thomae. Scaling of hard thermal turbulence in Rayleigh—Bénard convection. *Journal of Fluid Mechanics*, 204(1):1–30, 1989. doi: 10.1017/S0022112089001643.

[37] Hamid Karani and Christian Huber. Role of thermal disequilibrium on natural convection in porous media: Insights from pore-scale study. *Physical Review E*, 95(3), 3 2017. ISSN 24700053. doi: 10.1103/PhysRevE.95.033123.

[38] William M. Deen. *Analysis of transport phemomena*. Oxford University Press Inc., 1998.

[39] Roger Joseph Anna Janssen. *Instabilities in natural-convection flows in cavities*. PhD thesis, TU Delft, 1994.